Distribution Agreement

In presenting this thesis as a partial fulfillment of the requirements for a degree from Emory University, I hereby grant to Emory University and its agents the non-exclusive license to archive, make accessible, and display my thesis in whole or in part in all forms of media, now or hereafter now, including display on the World Wide Web. I understand that I may select some access restrictions as part of the online submission of this thesis. I retain all ownership rights to the copyright of the thesis. I also retain the right to use in future works (such as articles or books) all or part of this thesis.

Jack Li April 12, 2022

The Wave Equation and the Timpani: An Exploration into Various Models for the Vibration of a Timpani Drumhead

by

Jack Li

David Borthwick, PhD
Adviser

Mathematics

David Borthwick

Adviser

Alessandro Veneziani

Committee Member

Stephen Crist

Committee Member

2022

The Wave Equation and the Timpani: An Exploration into Various Models for the Vibration of a Timpani Drumhead

By

Jack Li

David Borthwick, PhD

Adviser

An abstract of
a thesis submitted to the Faculty of Emory College of Arts and Sciences
of Emory University in partial fulfillment
of the requirements of the degree of
Bachelor of Science with Honors

Mathematics

2022

Abstract

The Wave Equation and the Timpani: An Exploration into Various Models for the Vibration of a Timpani Drumhead

By Jack Li

The vibration of a timpani can be approximately modeled using the 2-dimensional wave equation, and various other factors (such as damping or viscoelastic effects) can also be quantitatively factored into the formulation of the equation.

Various initial conditions (specifying an initial displacement, an initial velocity, and various forcing terms) and versions of the wave equation were used to model the vibration of a kettledrum, and animations, periodograms of the vibration at the point of impact, and synthesized sounds using the point of impact were used to assess the accuracy of each model and the effects that each model had on the vibration of the drum. Moreover, points of impact were obtained from a survey response and their resulting animations, periodograms and sounds compared to the literature point of impact of 0.75r.

It was found that, with regards to initial conditions, while it was possible for the amplitudes of vibrational modes to change significantly between various choices of initial conditions (with a Dirac forcing term at 0.75r appearing to give the most accurate sound and vibration out of all chosen conditions), the frequencies of these modes did not seem to be significantly affected by these initial conditions. First-order damping also did not seem to significantly affect frequencies, and the impact of viscoelastic effects was similarly slight, only slightly raising the frequencies of higher frequency modes. These modeled frequencies all ended up being significantly higher than what was found in reality - it was deduced using results from Gallardo et. al 2020 and Fletcher et al. 1997 that the effect of air-loading, which was not accounted for in any of the equations, was responsible for this effect.

The Wave Equation and the Timpani: An Exploration into Various Models for the Vibration of a Timpani Drumhead

By

Jack Li

David Borthwick

Adviser

A thesis submitted to the Faculty of Emory College of Arts and Sciences
of Emory University in partial fulfillment
of the requirements of the degree of
Bachelor of Science with Honors

Mathematics

2022

Acknowledgements

Dr. David Borthwick has been an invaluable advisor throughout the process of this thesis - providing the inspiration for this project, guiding me when I got stuck, and helping provide a clear sense of structure to this online project.

I am grateful to Dr. Alessandro Veneziani for providing additional insight to the project, particularly regarding air loading and the Dirac nature of the forcing term.

I am grateful to Dr. Stephen Crist for feedback on the thesis defense, especially with regard to the context of where timpani are used in music.

I am grateful to Zoe Zimmerman for distributing the survey and collecting the responses, and thankful to those 8 drummers that responded as well, and Dr. Paul Bhasin for pointing me towards Zimmerman.

I am grateful to Dr. Bree Ettinger for insight on how to handle the received survey responses.

Table of Contents

The Wave Equation and the Timpani: An Exploration into Various Models for the Vibration of a Timpani Drumhead

Jack Li[1]

[1] **Emory University**

ABSTRACT

The vibration of a timpani can be approximately modeled using the 2-dimensional wave equation, and various other factors (such as damping or viscoelastic effects) can also be quantitatively factored into the formulation of the equation. Various initial conditions (specifying an initial displacement, an initial velocity, and various forcing terms) and versions of the wave equation were used to model the vibration of a kettledrum, and animations, periodograms of the vibration at the point of impact, and synthesized sounds using the point of impact were used to assess the accuracy of each model and the effects that each model had on the vibration of the drum. Moreover, points of impact were obtained from a survey response and their resulting animations, periodograms and sounds compared to the literature point of impact of 0.75r. It was found that, with regards to initial conditions, while it was possible for the amplitudes of vibrational modes to change significantly between various choices of initial conditions (with a Dirac forcing term at 0.75r appearing to give the most accurate sound and vibration out of all chosen conditions), the frequencies of these modes did not seem to be significantly affected by these initial conditions. First-order damping also did not seem to significantly affect frequencies, and the impact of viscoelastic effects was similarly slight, only slightly raising the frequencies of higher frequency modes. These modeled frequencies all ended up being significantly higher than what was found in reality - it was deduced using results from Gallardo et. al 2020 and Fletcher et al. 1997 that the effect of air-loading, which was not accounted for in any of the equations, was responsible for this effect.

Keywords: Wave Equation, Timpani, Modeling

Contents

List of Figures

List of Tables

1 INTRODUCTION

The timpani (also known as a kettledrum) is a widely used instrument across multiple genres of music, mostly notably music in the classical tradition and the repertoire of concert band - thus, it occupies a notable role in both symphony orchestras and wind ensembles. Moreover, the timpani can appear in digital music - in these instances, the sound is typically sampled from a real-life recording of a timpani.

1.1 The Closed-Form Solution for the 2-Dimensional Wave Equation

We can use mathematics to attempt to model a timpani after impact, as the motion of a timpani membrane is governed by mathematical equations: The resulting vibration of the drumhead of a timpani following an impact with a timpani mallet can be though of as a vibration of a circular membrane. This vibration of a circular membrane with radius a itself can be represented with a partial differential equation known as the 2-dimensional wave equation, the basic form of which is shown below:

$$u_{tt} = c^2(u_{xx} + u_{yy}), \tag{1}$$

Where u is a function of the displacement of the circular membrane at the point (x, y) at time t, u_{xx}, u_{yy} and u_{tt} represent the second partial derivative of u for x, y and t respectively, and c represents the propagation speed of the membrane (Nagata 2014, Slide 3). This propagation speed depends on the density of the membrane and the tension at which the membrane is at. Specifically, we have that

$$c^2 = \frac{T}{\rho}, \tag{2}$$

where T represents the tension of the membrane, and ρ the areal density of the membrane. (Borthwick 2017, pp. 45-47)

Moreover, the solution is restricted by the Dirichlet boundary conditions - that is, since we assume that the membrane (the drumhead of the timpani) is rigidly attached to a frame at its boundary, we can say that this membrane is incapable of movement - that is, $u(x, y, t) = 0$ wherever $\sqrt{x^2 + y^2} = 1$.

Finally, the solution this function takes on ultimately depends on two initial conditions - specifically, the initial shape of the membrane, and the initial velocity of membrane. These can be represented by functions $g(x, y)$ and $h(x, y)$ as follows:

$$g(x,y) = u(x,y,0) \tag{3}$$

$$\bar{h}(x,y) = u_t(x,y,0) \tag{4}$$

The existing of boundary and initial conditions means that this equation is an initial value boundary problem, of which there exists a classical solution, obtained by using separation of variables (Yong n.d. p. 2). First, x and y can be converted into polar coordinates to yield the wave equation based on r (the distance of the point from the origin) and θ (the angle between the vector from the origin to the point and the x-axis):

$$u_{tt} = c^2(u_{rr} + \frac{1}{r}u_r + \frac{1}{r^2}u_{\theta\theta}), \tag{5}$$

where $x = r\cos(\theta)$ and $y = r\sin(\theta)$.

Next, we can assume that (5) has a solution in which all the variables are separated, that is:

$$u(r,\theta,t) = R(r)\Theta(\theta)T(t), \tag{6}$$

where Ψ is some function only of the polar coordinates and T is some function only of time.

We can then substitute the separated form of u in (6) into (5), followed by division of both sides by $c^2R(r)\Theta(\theta)T(t)$ to obtain the new equation

$$\frac{T''(t)}{c^2T(t)} = \frac{R''(r)}{R(r)} + \frac{R'(r)}{rR(r)} + \frac{\Theta''(\theta)}{r^2\Theta(\theta)}. \tag{7}$$

Notably, we see that the left hand side depends only on t and the right hand side depends only on r and θ. By that logic, in order for equality to be achieved, both sides must be equal to some constant k.

We know this constant must be negative by Green's first identity applied to vector field $F = u\nabla u$ and V the 2-dimensional disk we are studying:

$$\int_V (u\Delta u + \nabla u \cdot \nabla u)dV = \oint_{\delta V} u\nabla u dS \tag{8}$$

.

By the Dirichlet condition, the right hand side must be equal to 0 (because $u = 0$ on $(x, y) = \delta V$, leaving:

$$\int_V (u\Delta u + \nabla u \cdot \nabla u) dV = 0 \tag{9}$$

and thus

$$\int_V (-u\Delta u) dV = \int_V (\nabla u \cdot \nabla u) dV \tag{10}$$

.

Given our manipulations of the original wave equation, we know that the right hand side of (7) is equal to $\frac{\Delta u}{u}$, thus we know this must be a constant, which implies that $\Delta u = ku$ for some constant k.

Therefore, we have that

$$-k \int_V (u^2) dV = \int_V (\nabla u \cdot \nabla u) dV \tag{11}$$

Given that we do not want the trivial solution, we know that the right side must be greater than zero, and therefore $-k \int_V (u^2) dV > 0$, and since the integrand u^2 is similarly always nonnegative, we obtain that $-k \int_V (u^2) dV > 0$, which implies that $k < 0$, meaning we can write k as $-\lambda^2$

Then, we obtain the equations

$$\frac{T''(t)}{c^2 T(t)} = -\lambda^2, \tag{12}$$

and

$$\frac{R''(r)}{R(r)} + \frac{R'(r)}{rR(r)} + \frac{\Theta''(\theta)}{r^2 \Theta(\theta)} = -\lambda^2. \tag{13}$$

From (8), the harmonic oscillator equation, we thus obtain that T takes the form $T = A\sin(c\lambda t) + B\sin(c\lambda t)$ for some constants A and B (Haber 2009, p. 1).

From (9), we can further separate the variables of this equation and multiply by r^2 to obtain

$$\lambda^2 r^2 + r^2 \frac{R''(r)}{R(r)} + r\frac{R'(r)}{R(r)} = -\frac{\Theta''(\theta)}{\Theta(\theta)}. \tag{14}$$

As with before, since the left hand side is entirely in the form of r and the right hand side is entirely in the form of θ, we have that both sides must be equal to a constant n^2. Therefore, using a solution analogous to that of solving T in (8), we get that $\Theta(\theta) = C\sin(n\theta) + D\sin(n\theta)$, where C and D are also constants.

Moreover, equating the left hand side to n^2 and multiplying by $R(r)$ yields the ordinary differential equation

$$(\lambda^2 r^2 - n^2)R(r) + r^2 R''(r) + rR'(r) = 0, \tag{15}$$

,

with the boundary condition that $R(a) = 0$, the solutions of which are known to be a linear combination of the Bessel functions of the first (J_n) and second kind (Y_n). Plots of the $n = 0$ through $n = 5$ of both types of functions are shown in Appendix G.

$$R(r) = EJ_n(\lambda r) + FY_n(\lambda r). \tag{16}$$

.

However, since $R(0)$ must be defined, and because Y_n has singularities at $r = 0$, we must have that $F = 0$, and therefore $R(r)$ must be a linear combination of the Bessel functions of the first kind.

Since we do not want the trivial solution of $E = 0$, the boundary condition that $R(a) = 0$ necessitates that each individual component of the Bessel functions be stretched so that $EJ_n(\lambda r) = 0$ at $r = a$.

Note that the Bessel functions themselves have multiple zeroes; thus, we can write $R(r)$ as a linear combination of Bessel functions of the first kind $E_{mn}J_n(\lambda_{mn}r$, where J_n is the nth Bessel function of the first kind, and $\lambda_{mn} = \frac{\alpha_{mn}}{a}$, where α_{mn} is the mth root of J_n, and E_{mn} some arbitrary constant.

1.2 Fourier-Bessel Expansion

Thus, as the above section derived, we have a general classical solution:

$$u(r,\theta,t) = \sum_{m=1}^{\infty}\sum_{n=0}^{\infty}(J_n(\lambda_{mn}r))(A_{mn}\cos(n\theta) + B_{mn}\sin(n\theta))(\cos(c\lambda_{mn}t) + \sin(c\lambda_{mn}t)),$$

where the constants A_{mn} and B_{mn} are determined by the initial conditions. Classically, these constants can be determined by the Fourier-Bessel expansion by component decomposition of the initial condition functions with the functions $J_n(\lambda_{mn}r)cos(n\theta)$ and $J_n(\lambda_{mn}r)sin(n\theta)$ - which form a complete orthogonal set for our inner product space of continuous functions in the continuous disk (Daileda 2012, Slide 9) - this is the case because each of these functions is product of a Bessel functions of the first kind - the collection of which form a complete orthogonal set in the radial dimension $(0, a)$ (Weisstein n.d.) - and $\cos(n\theta)$ or $\sin(n\theta)$, the collection of which form a complete orthogonal set in the angular dimension $(0, 2\pi)$.

Using this analysis, the function u can be split up into its normal modes (note that most constants have been normalized to 1):

$$u_{mn} = \sum_{m=1}^{\infty}\sum_{n=0}^{\infty} J_n(\lambda_{mn}r)(a_{mn}\cos(n\theta) + b_{mn}\sin(n\theta))\cos(c\lambda_{mn}t) \tag{17}$$

$$u^*_{mn} = \sum_{m=1}^{\infty}\sum_{n=0}^{\infty} J_n(\lambda_{mn}r)(a^*_{mn}\cos(n\theta) + b^*_{mn}\sin(n\theta))\sin(c\lambda_{mn}t), \tag{18}$$

To account for the initial conditions, we can set $t = 0$ to get the initial shape equation with respect to this expansion; we can also derive with respect to t to get the initial velocity equation with respect to this expansion:

$$g(r,\theta) = u(r,\theta,0) = \sum_{m=1}^{\infty}\sum_{n=0}^{\infty} J_n(\lambda_{mn}r)(a_{mn}\cos(n\theta) + b_{mn}\sin(n\theta)) \tag{19}$$

$$h(r,\theta) = u_t(r,\theta,0) = c\lambda_{mn}\sum_{m=1}^{\infty}\sum_{n=0}^{\infty} J_n(\lambda_{mn}r)(a^*_{mn}\cos(n\theta) + b^*_{mn}\sin(n\theta)), \tag{20}$$

In the former case, setting $t = 0$ removes the $sin(c\lambda_{mn}t)$ components, meaning that g is determined entirely by a_{mn} and b_{mn}, while in the latter case, setting $t = 0$ and deriving with respect to t removes the $cos(c\lambda_{mn}t$ components, meaning that h is determined entirely by a^*_{mn} and b^*_{mn}.

Then we have that the coefficients a_{mn} and b_{mn} are determined by the initial shape function g (which itself must be converted into polar coordinates) by

$$a_{m0} = \frac{1}{\pi a^2 J_{n+1}^2(\alpha_{m0})} \int_0^{2\pi} \int_0^a g(r,\theta) J_n(\lambda_{mn} r) \cos(n\theta) r dr d\theta \tag{21}$$

$$a_{mn} = \frac{2}{\pi a^2 J_{n+1}^2(\alpha_{mn})} \int_0^{2\pi} \int_0^a g(r,\theta) J_n(\lambda_{mn} r) \cos(n\theta) r dr d\theta \tag{22}$$

$$b_{m0} = \frac{1}{\pi a^2 J_{n+1}^2(\alpha_{m0})} \int_0^{2\pi} \int_0^a g(r,\theta) J_n(\lambda_{mn} r) \sin(n\theta) r dr d\theta \tag{23}$$

$$b_{mn} = \frac{2}{\pi a^2 J_{n+1}^2(\alpha_{mn})} \int_0^{2\pi} \int_0^a g(r,\theta) J_n(\lambda_{mn} r) \sin(n\theta) r dr d\theta, \tag{24}$$

and where the coefficients a^*_{mn} and b^*_{mn} are determined by the initial velocity condition function h (also converted into polar coordinates) by

$$a^*_{mn} = \frac{1}{\pi c \alpha_{m0} a J_{n+1}^2(\alpha_{m0})} \int_0^{2\pi} \int_0^a h(r,\theta) J_n(\lambda_{mn} r) \cos(n\theta) r dr d\theta \tag{25}$$

$$a^*_{mn} = \frac{2}{\pi c \alpha_{mn} a J_{n+1}^2(\alpha_{mn})} \int_0^{2\pi} \int_0^a h(r,\theta) J_n(\lambda_{mn} r) \cos(n\theta) r dr d\theta \tag{26}$$

$$b^*_{mn} = \frac{1}{\pi c \alpha_{m0} a J_{n+1}^2(\alpha_{m0})} \int_0^{2\pi} \int_0^a h(r,\theta) J_n(\lambda_{mn} r) \sin(n\theta) r dr d\theta \tag{27}$$

$$b^*_{mn} = \frac{2}{\pi c \alpha_{mn} a J_{n+1}^2(\alpha_{mn})} \int_0^{2\pi} \int_0^a h(r,\theta) J_n(\lambda_{mn} r) \sin(n\theta) r dr d\theta. \tag{28}$$

Each of these coefficients is the result of a (normalized) inner product of one of the initial condition functions with one of the components of the complete orthogonal set mentioned above, the sum of which makes up a component decomposition of each of these functions.

1.3 Vibrational Modes

These coefficients correspond to the contribution of individual "vibrational modes" to the overall motion of the membrane - each with their own characteristic shape and frequency - for example, the (3,2) mode is obtained from $n = 3, m = 2$. It has been found previously that the (1,1), (2,1), (3,1), (4,1) and (5,1) modes, due to the ratios of their frequencies in a timpani (which are quite similar to 2:3:4:5:6) are the ones most relevant to the harmonic pitch of the kettledrum when struck (Fletcher and Rossing 1997, p. 584) - this 2:3:4:5:6 ratio is harmonic due to the ratios of the frequencies relative to each other: in musical terms, a 3:2 ratio is a perfect fifth, a 4:3 ratio is a perfect fourth, a 5:4 ratio is a major third, and a 6:5 ratio is a minor third. (Müller n.d.)

Figures 1-5 represent a frame from an animation of each of these relevant vibrational modes - the full

animations can be found in the Acoustics and Vibration Animations webpage of Dan Russell's (Grad. Prog. Acoustics, Penn State) websites. (Russell 2018):

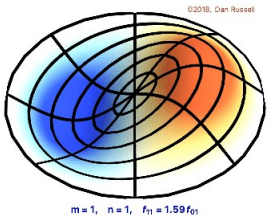

Figure 1. (1,1) mode

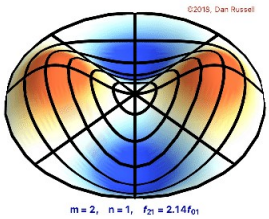

Figure 2. (2,1) mode

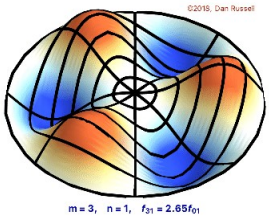

Figure 3. (3,1) mode

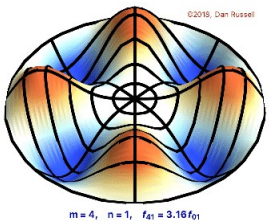

Figure 4. (4,1) mode

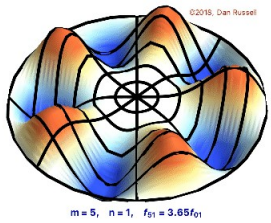

Figure 5. (5,1) mode

Importantly, the location at which the timpani is struck can influence the individual intensity of each of these vibrational modes - It has been demonstrated that as the point of impact moves away from the center of the drum (starting at 5/12 the radius away from the center and ending at 8/12 the radius), while the (1,1), (2,1) and (3,1) modes do not change significantly in intensity, the (4,1) mode decreases in intensity while the (5,1) mode increases in intensity (Y. Nishimura and S. Nishimura 2015, p. 47). Moreover, as an extreme case, Yong notes that striking a drum exactly at the center only excites those modes with $n = 0$, with any other vibrational modes completely excluded. (Yong n.d. p. 4)

1.4 Limitations of the Standard Model

However, in reality, the standard 2-dimensional wave equation leaves out several critical components of a drum: firstly, due to the existence of friction, the motion of the drumhead will be damped over time, which, as Yong points out, may change the coefficients of the vibrational modes and their frequencies. (Yong n.d. p. 5) Therefore, using the Fourier-Bessel expansion in this manner is not a viable strategy should we want a damped model of drumhead vibration.

In addition, there are also viscoelastic effects that play a role in the model - the standard 2-dimensional wave equation assumes a purely elastic membrane and does not account for the ability of the membrane to resist deformation/strain from a stress, such as the impact of a mallet on the membrane, with respect to time - Wang 2016 specifies a model accounting for such effects later. (Wang 2016, pp. 1216–1217)

Other factors that can also have an effect on the vibration of the membrane is the bending stiffness of the membrane - that is, the resistance of the membrane towards bending (which is assumed to be zero in the standard equation), which must be accounted for by a fundamentally different equation - that of thin plate vibration. In addition, the standard wave equation assumes that each point in the membrane vibrates straight up and down, which is assumption that cannot be made in a real drum. Another important effect is that of air-loading: the membrane of a timpani is typically stretched over a kettle that is loaded with air, which can lead to pressure differences above and below the membrane as it vibrates, also influencing its vibration.

1.5 Numerical Methods: The Finite Element Method

While it may still be possible to determine an analytic solution for the damped 2-dimensional wave equation $u_{tt} + \rho u_t = c^2(u_{xx} + u_{yy})$ (where ρ represents the coefficient of friction) and the various other modifications to the model, and then perform Fourier-Bessel expansion on this new classical solution, it may be more practical instead to move towards a numerical solution.

One effective numerical approach is the finite element method, which can be performed in Wolfram Mathematica provided we provide it with a partial differential equation to solve, any relevant boundary conditions, the necessary initial conditions (in this case we can use an initial shape g and initial velocity condition h), and a discretization of the region we want to solve the partial differential equation on (that is, a "mesh") of the region.

Then, after specification of the equation, appropriate initial and boundary conditions, and an appropriate mesh for the region, and specific region of time, the command NDSolveValue in Mathematica provides us with a numerical approximate solution for the function by using the finite element method to determine values on each finite element of the mesh for each time step, and to then connect these values by interpolation.

In spite of the lack of differentiability that comes with linear interpolation, it is well-known and can be demonstrated that these finite element approximations converge to the exact solution as the mesh gets refined, although the details of this proof are beyond the scope of this paper. (Ham and Cotter 2014).

In addition, important to note is that any digital recording or sample meant to emulate a drum only represents one of many possible sound outcomes that can be produced by hitting a timpani - in reality, professional drummers do not all aim to exactly hit a quarter of the way from the edge of the membrane - there can be often significant variation between drummers in where they strike, which may also affect the sound and vibration of the drum, and even variation between the same drummer.

2 METHODS AND MATERIALS

Six partial differential equation models (Mallet Radius, Initial Displacement, Initial Velocity, Forced, Forced with Modified Wave Equation, and Forced with Modified Wave Equation with Dirac-like elements), differing in initial conditions and equations, each a refinement of the model before it, were attempted to model the impact of a mallet on the drumhead of a timpani.

The specifications of the timpani we are attempting to model can be found in Gallardo et. al 2020 - the timpani we are attempting to model is that of a Adams Renaissance 32 inch drumhead - the radius of the drumhead is .4015 meters, with a membrane tension of 3600N and an areal membrane density of .262 kg/m^2. (Gallardo et al. 2020, p. 10)

This membrane tension and density thus corresponds to a propagation speed of $c = \sqrt{\frac{3600}{.262}} = 117.22 m/s$

Research from Rossing et. al 1982 found that the "normal" place to strike the drum (that is, the location that produces the highest intensity of the above-mentioned vibrational modes and minimizes the presence of other more dissonant vibrational frequencies, such as the (1,2) or (0,2) modes) was approximately a quarter of the way from the edge of the drum (Rossing 1982, p. 175) - thus, the subsequent PDE models take the point of impact three-quarters from the center. Since the drum is presumed to be rotationally symmetric, any point satisfying this requirement can be selected - thus, for simplicity, the point of impact was specified to be $(.75 * .4015, 0) = (.301125, 0)$.

For the Initial Displacement, Initial Velocity, Forced Model, and Forced Model with Modified Wave Equation, a "conical" surface was used as part of either initial velocity or shape condition, the approximate equation and algorithm of which is described below:

1. First, for any given point (x, y) and maximal point $(a = .75 * .4015, 0)$, define the parametric equation

$$q(t) = t(x, y) + (1 - t)(a, 0). \tag{29}$$

   This function corresponds to the line connecting $(a, 0)$ and (x, y) where $q(0) = (a, 0)$ and $q(1) = (x, y)$.

2. Then, we wish to find t_0 such that $\|q(t_0)\|^2 = .4015^2$. This is a quadratic equation with two different solutions, one of which is positive and the other of which is negative - for simplicity, we will use the positive root, and define this as t_0

3. If we do this, then we can define the conical function's value at (x, y) to be $1 - 1/t_0$, and we define the conical function's value at $(a, 0)$ to be 1.

4. the end result is a conical function where the function is at its maximum of 1 at $(a, 0)$, the function is 0 at the boundary of the membrane.

   Moreover, any given point (x, y) inside the membrane not equal to the maximal point will fall on a single line segment from $(a, 0)$ to some point on the edge of the membrane b. Then the value of the conical function at (x, y) is equal to $\frac{d_1}{d_2}$, where d_1 is the distance from (x, y) to b, and d_2 is the distance between $(a, 0)$ and b.

Ultimately, the (approximate) equation of the conical function $conical(x, y)$ is given by

$$conical(x,y) = 1 - \frac{5.8*10^6 - 3.9*10^7 x + 6.4*10^7 x^2 + 6.4*10^7 y^2}{5.8*10^6 - 1.9*10^7 x + 0.07\sqrt{1.2*10^{16} - 8.1*10^{16} x + 1.3*10^{17} x^2 + 5.9*10^{16} y^2}} \quad (30)$$

with the parametric plot of the function given by Figure 6.

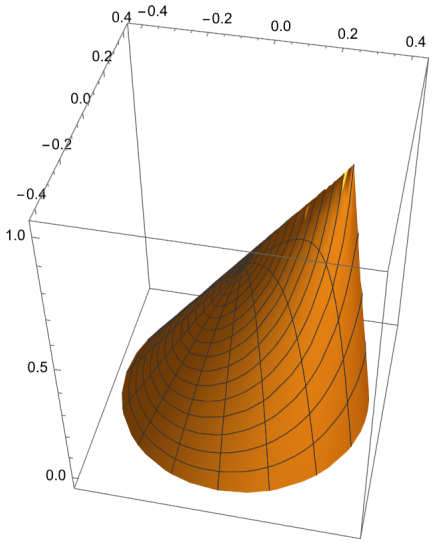

Figure 6. parametric 3D plot of $conical(x,y)$

This function can be scaled as needed to match the appropriate values for the initial velocity and shape conditions - for example, in all cases, the impact was modeled as a downward strike, requiring a negative scaling factor.

All models followed the same Dirichlet boundary condition for a rigid circular membrane that $u(x,y,t) = 0$ for $\sqrt{x^2+y^2} = 1$. With the exception of the first model (the mallet radius model), in which we were still working towards refining the conditions of the method, all coefficients for the initial conditions and wave equations were selected to have an approximate final maximum displacement of at least 0.01m but at most 0.05m, and a vibration phase that lasted approximately 3 seconds.

2.1 The Mallet Radius Model

Using the initial assumption that the mallet would only directly immediately affect the region of the drumhead that it makes contact with, a model was proposed using the damped wave equation with a flat initial shape equation and an initial velocity equation with a rapid downwards velocity in the region that the mallet makes contact with, shaped like a parabolic curve - this was meant as a simulation of the Dirac delta function used for a point impulse that also accounted for the reality of the mallet.

The radius of the mallet was based on a Vic Firth T1 timpani mallet, and set to be 0.75 inches (corre-

sponding to .01905m).

The PDE used was as follows:

$$u_{tt} + 0.6c^2 u_t = c^2(u_{xx} + u_{yy}) \tag{31}$$

NOTE: the friction coefficient being very high in this instance led to very quick dissipation in this model.

The initial shape equation used was as follows:

$$u(0, x, y) = g(x, y) = 0 \tag{32}$$

The initial velocity equation used was as follows:

$$\frac{\partial u}{\partial t}(0, x, y) = h(x, y) \tag{33}$$

where $h(x, y) = \frac{100(.01905^2 - ((x - .301125)^2 + y^2)}{.01905^2}$ for (x, y) within the circle centered at $(.301125, 0)$ with radius .01905, and 0 otherwise.

The mesh, which was set to have a maximum cell measure of 0.0001, consisted of 7890 triangular elements. The actual appearance will be shown in Appendix A.

2.2 The Initial Displacement Model

The initial displacement model was generated using a visualization of what the drum would look like at the point of maximal displacement once impacted: similar to how the plucking of a string on a string instrument creates an initial triangular function (Russell 2020), it was assumed that at the analogous time of "maximal displacement" following mallet impact that the displacement of the drumhead would similarly resemble that of a conical function with 0 velocity as the tension caused it to recoil back.

The PDE used was $u_{tt} + .0005c^2 u_t = c^2(u_{xx} + u_{yy})$, the initial shape equation used was $equationu(0, x, y) = g(x, y) = -.05conical(x, y)$, and the initial velocity equation used was $\frac{\partial u}{\partial t}(0, x, y) = h(x, y) = 0$.

The mesh, which was set to have a maximum cell measure of 0.001, consisted of 806 triangular elements. The actual appearance will be shown in Appendix A.

2.3 The Initial Velocity Model

The third approach used a different model for the initial conditions: rather than only concentrating a sharp velocity within a small region or trying to pre-specify a potentially inaccurate initial displacement, this model began with a flat membrane, and imparted a velocity across the entire membrane that was larger near the point of impact, largest at the exact point of impact, and 0 at the boundary - this lent itself well to the use of a scaled conical function.

The PDE used was $u_{tt} + 0.00025c^2u_t = c^2(u_{xx} + u_{yy})$, the initial shape equation used was $u(0,x,y) = g(x,y) = 0$, and initial velocity equation used was $\frac{\partial u}{\partial t}(0,x,y) = h(x,y) = -15conical(x,y)$.

The mesh, which was set to have a maximum cell measure of 0.001, consisted of 806 triangular elements, just like with the initial displacement model. The actual appearance will be shown in Appendix A.

2.4 The Forced Model

The fourth approach acknowledged that the mallet would be in contact with the drum membrane for a short but nonzero period of time, and thus used two separate PDEs corresponding to a "forced phase" of vibration where the mallet is making contact with the membrane, and a "free phase" of vibration where the mallet is released from the membrane and the membrane is allowed to vibrate freely with the initial shape and velocity attained at the end of the forced phase.

Wagner 2006 studied the contact time of a drumstick on a drumhead and found that the contact time of the first impact was about 3.5 ms (with later reflections of the vibration coming in shortly after contributing to further impacts, but that will be omitted from this model for simplicity) (Wagner 2006, pp. 21–22). Therefore, the "forced phase" lasted from $t = 0 to 3.5$ ms, and the "free phase" followed.

To accomplish this, different equations were set up for both phases: the forced term would have a "forcing term" meant to model the contact between the drumhead and the mallet, while the free phase would be the damped wave equation as usual. When deliberating the choice of forcing term, it was decided that the forcing term would need to be largest at the point of impact, larger near the point of impact, and 0 at the boundary. Thus, once again, a scaled conical term was used.

The PDEs used were as follows:

$$\frac{\partial^2}{\partial t^2}u_{forced} + \frac{30}{.0036}conical(x,y) + .00025\frac{\partial}{\partial t}u_{forced} = c^2(\frac{\partial^2}{\partial x^2}u_{forced} + \frac{\partial^2}{\partial y^2}u_{forced}) \tag{34}$$

$$\frac{\partial^2}{\partial t^2}u_{free} + .00025\frac{\partial}{\partial t}u_{free} = c^2(\frac{\partial^2}{\partial x^2}u_{forced} + \frac{\partial^2}{\partial y^2}u_{forced}). \tag{35}$$

The initial shape equations used were as follows:

$$u_{forced}(0,x,y) = g_{forced}(x,y) = 0 \tag{36}$$

$$u_{free}(.0035,x,y) = g_{free}(x,y) = u_{forced}(.0035,x,y). \tag{37}$$

The initial velocity equations used were as follows:

$$\frac{\partial}{\partial t}u_{forced}(0,x,y) = h_{forced}(x,y) = 0 \tag{38}$$

$$\frac{\partial}{\partial t}u_{free}(.0035,x,y) = h_{free}(x,y) = \frac{\partial}{\partial t}u_{forced}(.0035,x,y). \tag{39}$$

The forced phase mesh was set to have a maximum cell measure of .0005, and consisted of 1566 triangular elements. The free phase mesh was set to have a maximum cell measure of 0.0012, and consisted of 682 triangular elements. The actual appearances of these meshes will be shown in Appendix A.

2.5 The Forced, Modified Wave Equation Model

Wang 2016 describes an alternative form of the generalized wave equation based on viscoelastic effects as modeled by the Kelvin-Voigt equation - the effect of this modification is to replace the damping term from the standard first partial derivative term with respect to time with the Laplacian of this term, in essence converting the damping from a first-order term to a third-order term. (Wang 2016, p. 1217)

The fifth approach used this modified wave equation and adapted it into the force model used above. This modified damping term also necessitated a much smaller coefficient.

The PDEs used were as follows:

$$\frac{\partial^2}{\partial t^2}u_{forced} + \frac{30}{.0036}conical(x,y) = c^2\left(\frac{\partial^2}{\partial x^2}u_{forced} + \frac{\partial^2}{\partial y^2}u_{forced} + \frac{1}{200000}\Delta\frac{\partial}{\partial t}u_{forced}\right) \tag{40}$$

$$\frac{\partial^2}{\partial t^2}u_{free} = \frac{\partial^2}{\partial x^2}u_{free} + c^2\left(\frac{\partial^2}{\partial y^2}u_{free} + \frac{1}{200000}\Delta\frac{\partial}{\partial t}u_{free}\right). \tag{41}$$

The initial shape and initial velocity equations used were the same as with the forced model - a flat initial membrane and no initial movement. The initial shape and velocity conditions of the free phase were analogous to that of the forced model - to preserve continuity, they were set to equal the displacement and velocity at the end of the forced phase.

The forced phase mesh was set to have a maximum cell measure of .0005, and consisted of 1566 triangular elements. The free phase mesh was set to have a maximum cell measure of 0.002, consisted of 402 triangular

elements. The actual appearances of these meshes will be shown in Appendix A.

2.6 Adding a "Dirac"-like Element to The Forced, Modified Wave Equation Model

Under the consideration that the region directly under the mallet or very near the mallet may experience a much greater force than regions not under the mallet, the initial force was split into two components: the conical component as before, and a new "Dirac"-like component highly concentrated in a small circle centered at the point of impact.

The Dirac term was modeled using an multi-dimensional exponential function centered at and concentrated around the point of impact, with the formula $dirac[x,y] = -e^{(-5/.01905)((x-.75*.4015)^2+y^2)}$. .01905 was picked due to being the mallet radius, and the coefficient of 5 was selected to ensure that the boundary values could remain as close to 0 as possible.

3 different conditions were tried with this forcing term: "mostly conical", where the conical term had a larger coefficient than the Dirac term, "mostly Dirac", where the Dirac term had a larger coefficient than the conical term, and "purely Dirac" that had only the Dirac term.

The PDEs used were as follows:

Each model had the same "free phase" equation of

$$\frac{\partial^2}{\partial t^2}u_{free} = c^2(\frac{\partial^2}{\partial x^2}u_{free} + \frac{\partial^2}{\partial y^2}u_{free} + \frac{1}{200000}\Delta\frac{\partial}{\partial t}u_{free}) \tag{42}$$

. However, the mostly conical, mostly Dirac, and purely Dirac models differed in the forcing term used in their "forced phase":

$$\frac{\partial^2}{\partial t^2}u_{forced} + mostlyconical(x,y) = c^2(\frac{\partial^2}{\partial x^2}u_{forced} + \frac{\partial^2}{\partial y^2}u_{forced} + \frac{1}{200000}\Delta\frac{\partial}{\partial t}u_{forced}) \tag{43}$$

$$\frac{\partial^2}{\partial t^2}u_{forced} + mostlyconical(x,y) = c^2(\frac{\partial^2}{\partial x^2}u_{forced} + \frac{\partial^2}{\partial y^2}u_{forced} + \frac{1}{200000}\Delta\frac{\partial}{\partial t}u_{forced}) \tag{44}$$

$$\frac{\partial^2}{\partial t^2}u_{forced} + purelydirac(x,y) = c^2(\frac{\partial^2}{\partial x^2}u_{forced} + \frac{\partial^2}{\partial y^2}u_{forced} + \frac{1}{200000}\Delta\frac{\partial}{\partial t}u_{forced}), \tag{45}$$

where

$$mostlyconical(x,y) = 5000conical(x,y) + 2000dirac(x,y) \tag{46}$$

$$mostlydirac = 2000conical(x,y) + 5000dirac(x,y) \tag{47}$$

$$purelydirac = 35000dirac(x,y). \tag{48}$$

The initial shape and initial velocity equations used for all models were the same as with the forced and modified force model - a flat initial membrane and no initial movement, and the forced phase used the same mesh as the initial forced model's forced phase. The free phase was analogous to the force model's free phase as mentioned above. The mesh used for free vibration was set to have a maximum cell measure of .005, consisting of 202 triangular elements.

2.7 The Dirac-Forced, Modified Wave Equation Model applied to Surveyed Impact Points

A sample of $n = 8$ responses was collected by Zoe Zimmerman from drummers from Emory University Symphony Orchestra, Emory Youth Orchestra, and select percussionists outside of Emory yielded the histogram in Figure 7:

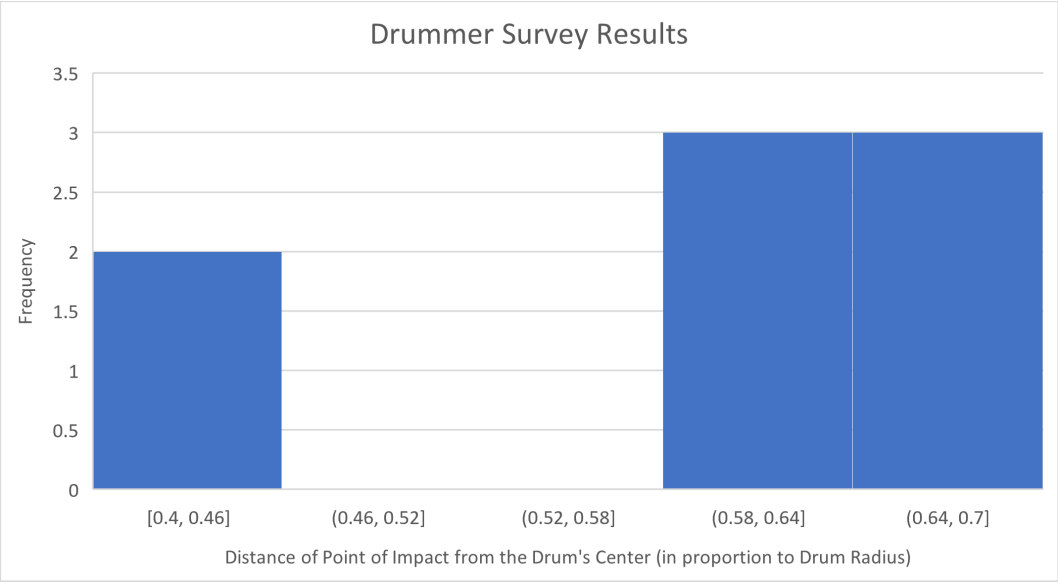

Figure 7. Drummer Survey Results

Treating the two separate clusters ($n = 2$ centered around 0.425 and $n = 6$ centered around 0.65) as their own distributions, the average values of $0.425r$ and $0.642r$ were then used as the radii for the point of impact in lieu of $0.75r$ supplied by literature. These new points of impact were then adapted to the purely Dirac modified force model - specifically, the initial forcing Dirac term was set to be centered around those points

instead, while all other conditions (such as mesh coarseness, free vibration, shape and velocity equations, etc. were held constant)

3 RESULTS

3.1 Animation Diagrams

Applying NDSolveValue to each of the models with the conditions specified above yielded a function $u(x, y, t)$ with values calculated within specific elements of the mesh by the finite element method implicit within NDSolveValue and the remaining values in the domain linearly interpolated with respect to these elements.

The function at each point in time can be plotted in 3D using the Plot3D function of Mathematica - several of these 3D plots at different time points could be assembled into a table of frames using the Table function.

Then, the ListAnimate function was used to convert this table into an animation, which could be exported as a GIF, with the 3D plot at each time point representing a frame of the animation.

Figure 8 shows one frame of animation from the purely Dirac modified force model with impact at 0.75r. A frame of animation from other models can be seen in Appendix B.

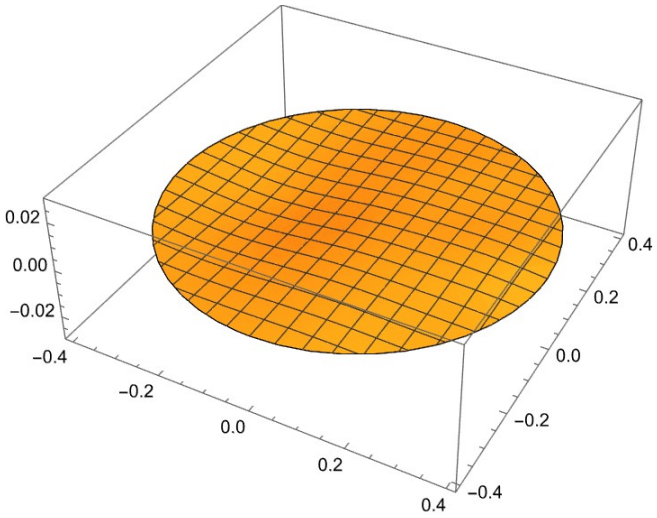

Figure 8. One frame of animation from the vibration of the purely Dirac modified force model at 0.75r

These animations were also compared to a YouTube video of a timpani vibration (Kréemes 2019).

3.2 Periodograms

For every model except the mallet radius model, a function $f(t)$ was created where $f(t) = u(.4015r, 0, t)$, where $(.4015r, 0)$ represents the point of impact used for the model, which was $r = 0.75$ except for the surveyed points of impact.

From this, a table of values of $f(t)$ was created from $t = 0$ to $t = 3$ seconds every 0.0000226 seconds, corresponding to a sample rate of approximately 44,248 Hz (this number was selected to best emulate the standard sampling rate of 44.1 kHz of audio).

For the forced models, two tables needed to be created, one for the "forced phase" and one for the "free phase".

The resulting function value tables were then flattened into a vector using the Flatten function (this could also flatten both forced phase + free phase tables into one vector). Using this, a periodogram of the vector can be created using Mathematica's Periodogram function - the sample rate was set to 44,248 Hz to match the sample rate of the table, and only frequencies from 0 to 600 Hz were displayed. In addition, audio was imported from Gallardo et al. 2020 of a recording of a timpani tuned to A2 (Gallardo et al. 2020, p. 10) - this audio similarly had the Periodogram function applied to it.

Figure 9 shows an example of a periodogram obtained this way for the purely Dirac modified force model with impact at 0.75r. The periodograms of other models and the recording are located in Appendix C.

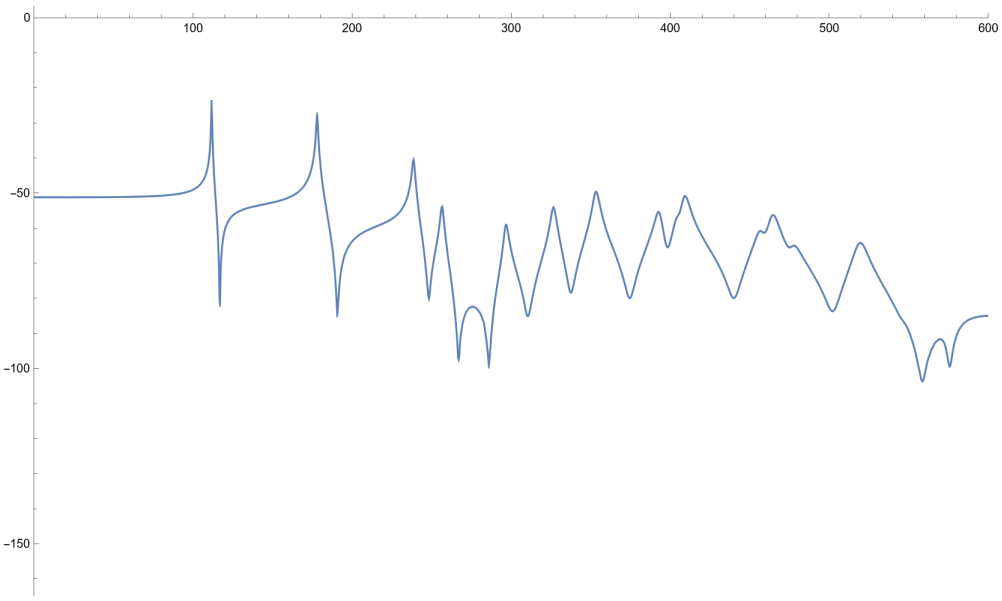

Figure 9. Periodogram of the purely dirac modified force model at 0.75r

3.3 Synthesized Sounds and Audio Waveforms

The flattened vector that was used to generate the periodogram could similarly to be used to generate a sound by use of the SampleSoundList function of Mathematica. The flattened vector was multiplied by a scalar modifier as needed to obtain an appreciable volume, and the sample rate was set to 44,248 Hz.

Using these synthesized and recorded sounds, the AudioPlot function was applied to these sounds to generate a waveform of the audio, all of which were then roughly scaled such that the loudest point

corresponds to 1 on the waveform graph. Figure 10 shows an example of a waveform obtained this way for the purely Dirac modified force model with impact at 0.75r. The waveforms of other models and the imported real sound are located in Appendix D.

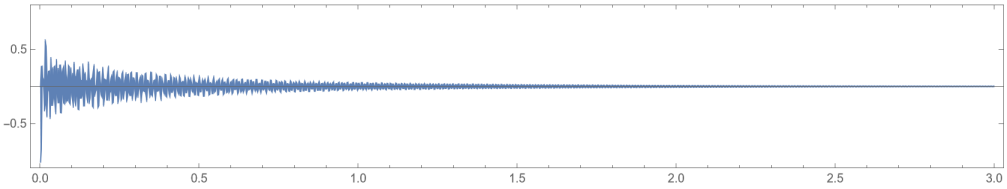

Figure 10. Waveform of the purely Dirac modified force model at 0.75r

3.4 Frequencies and Relative Amplitudes of Modes

Using the periodograms above, the frequencies and amplitudes of various vibrational modes for each model could be identified using the "Get Coordinates" functionality of Mathematica.

The frequencies could then be compared to the theoretical undamped frequencies predicted by the standard 2D wave equation, as articulated in the later subsection "Comparison of Frequencies to the Undamped Wave Equation".

The amplitudes obtained from each model were also normalized such that the largest amplitude mode (which was invariably (0,1) for all models) was set to 0 dB, the results of which are shown in Figure 11.

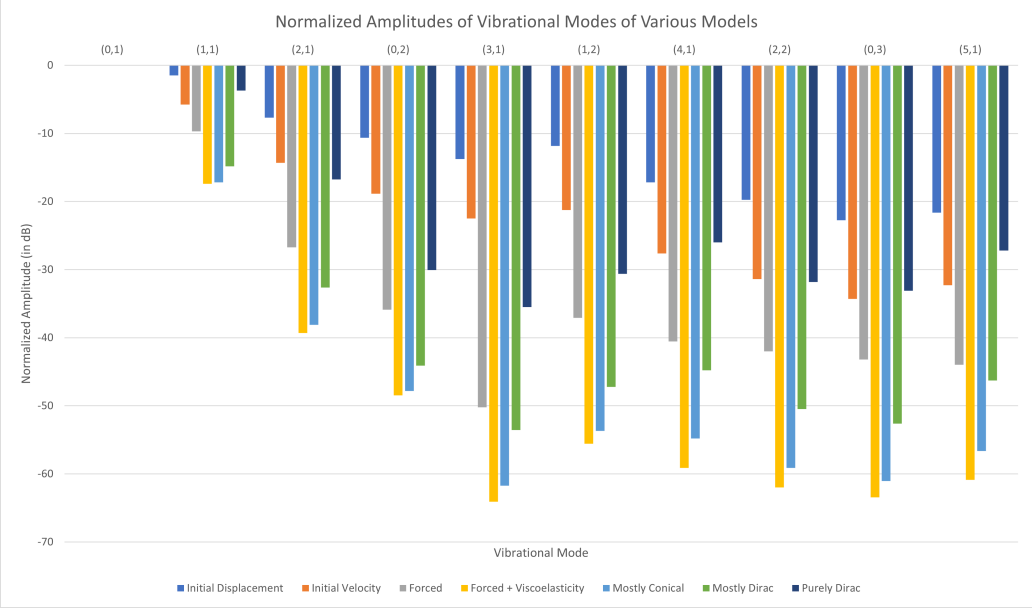

Figure 11. Normalized Amplitudes of Vibrational Modes of Various Models

3.5 Examining the Forced Model on Drummer Survey Results

Figure 12 shows the periodogram of the Dirac modified model with a point of impact at $0.642r$, and Figure 13 shows a similar model with a point of impact set at $0.425r$ instead.

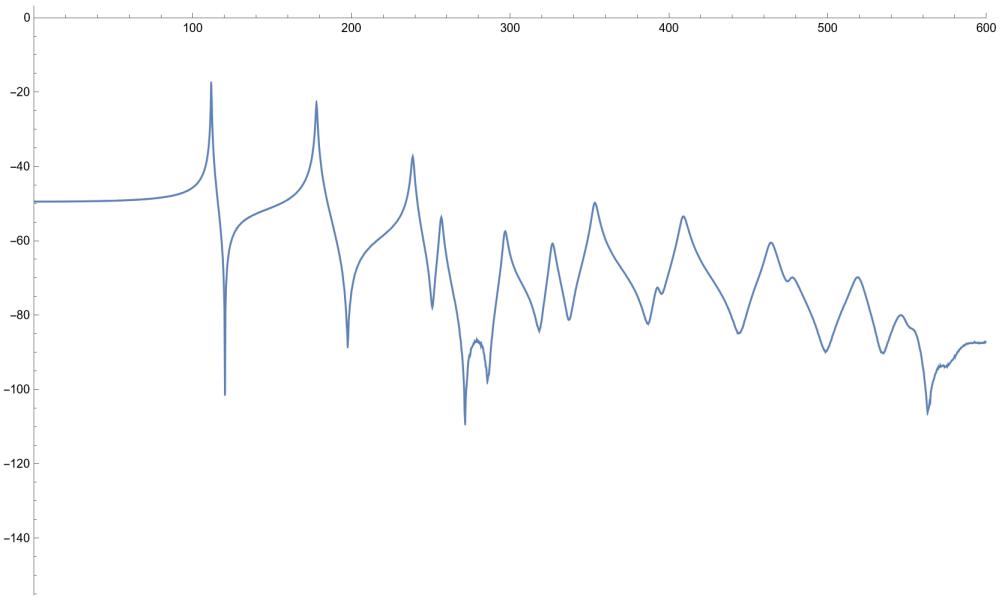

Figure 12. Periodogram of the purely dirac modified force model at 0.642r

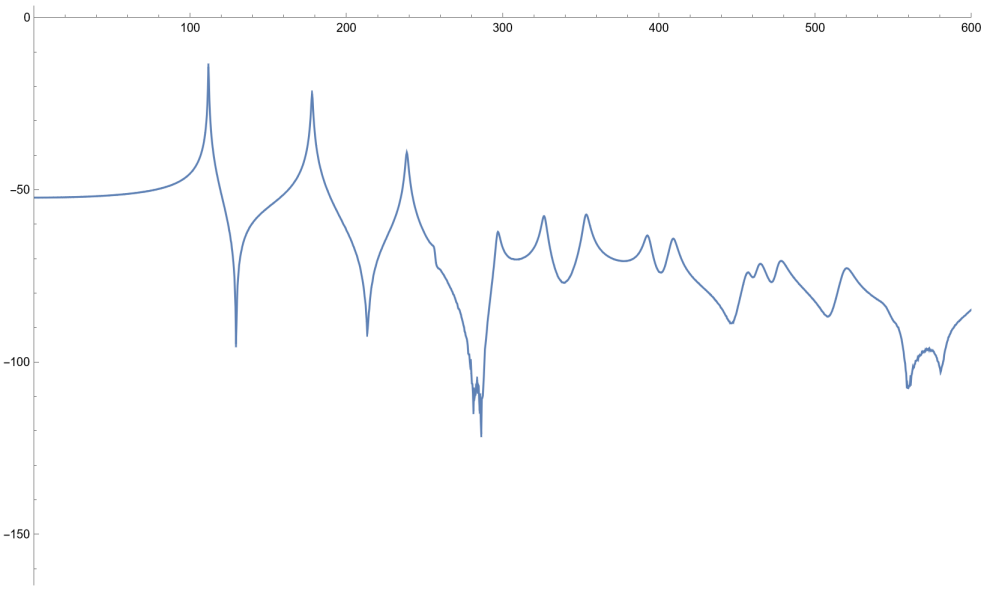

Figure 13. Periodogram of the purely dirac modified force model at 0.425r

Figure 14 shows the % difference between the frequency of the various vibrational modes of specifying the point of impact at $0.642r$ and $0.425r$ rather than the standard $0.75r$, while Figure 15 shows the normalized amplitudes of these modes with different survey-specific points of impact rather than the usual $0.75r$.

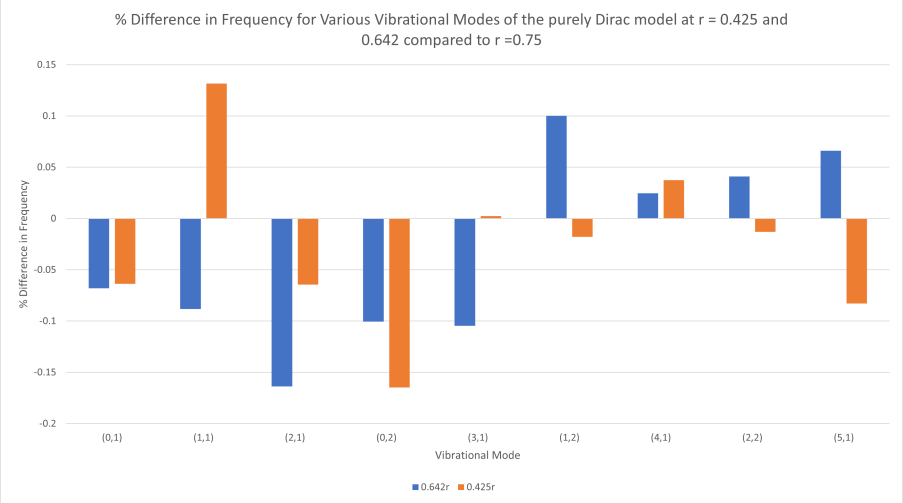

Figure 14. % Difference of Various Vibrational Modes of the purely Dirac model at 0.425r and 0.642r compared to 0.75r

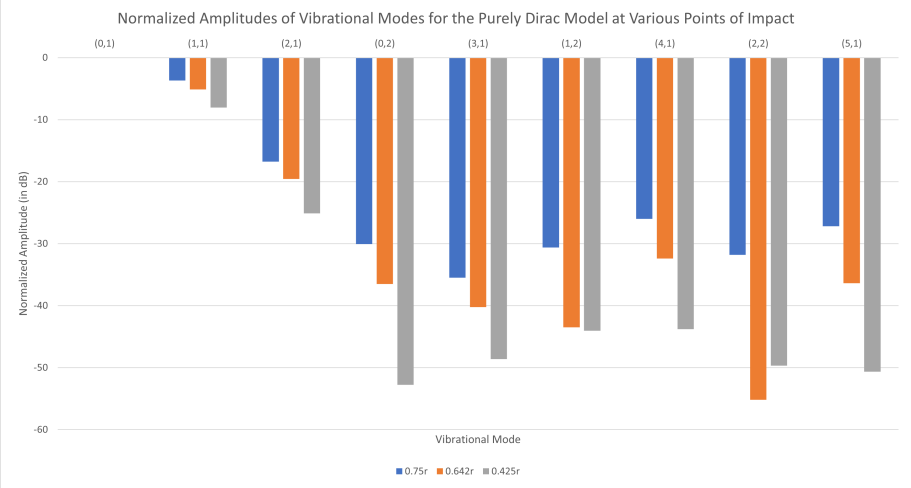

Figure 15. Normalized Amplitudes of Various Vibrational Modes for the purely Dirac models at Various Points of Impact

An important note: in the 400-410 Hz region, where most other periodograms show two peaks, one roughly corresponding to 405-406 Hz (the (0,3) mode) and the other corresponding to 408-409 Hz (the (5,1) mode), only one peak could be detected in this region corresponding to the latter. Therefore, we say that the (0,3) mode is "not detected" and thus does not appear in the figures showing % differences and normalized amplitudes.

3.6 Comparison of Frequencies to the Undamped Wave Equation

As we recall, each component of summation making up the general classical solution to the undamped wave equation $u_{tt} = c^2(u_{xx} + u_{yy})$ has an independent time-dependent component $A\cos(c\lambda_{mn}t) + B\sin(c\lambda_{mn}t)$ - this

can be used to determine the expected frequencies of the various vibrational modes of the undamped wave equation using the formula $f_{expected} = \frac{2\pi}{c\lambda_{mn}}$, where λ_{mn} is the n^{th} zero of the m^{th} order Bessel function of the first kind divided by the radius (in this case .4015). These expected frequencies were then compared to the calculated frequencies for the vibrational modes of each of the models, with the % difference between the undamped mode and the mode of each model shown in Figure 16. The raw frequencies for each model can be found in Appendix E.

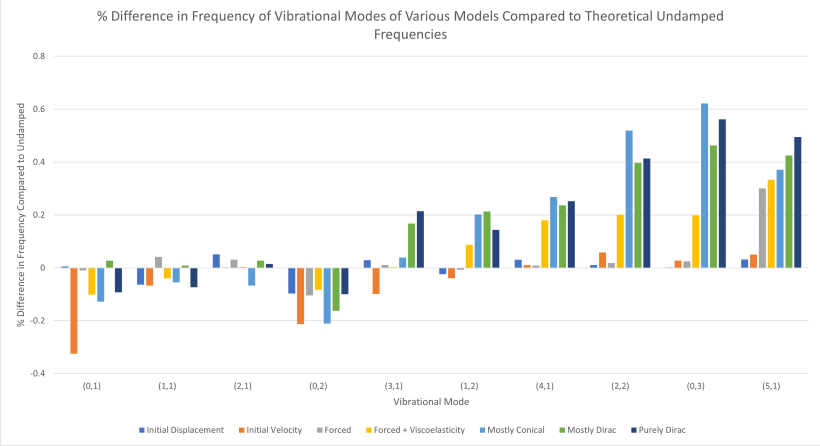

Figure 16. Percent Difference in Frequencies of Vibrational Modes of Various Models Compared to Theoretical Undamped Frequencies

In addition, these theoretical undamped frequencies can be compared to the frequencies found from a sample of real drum audio with the same conditions, obtained from Gallardo et. al 2020, as shown in Figure 17. The raw frequencies for each model can be found in Appendix E.

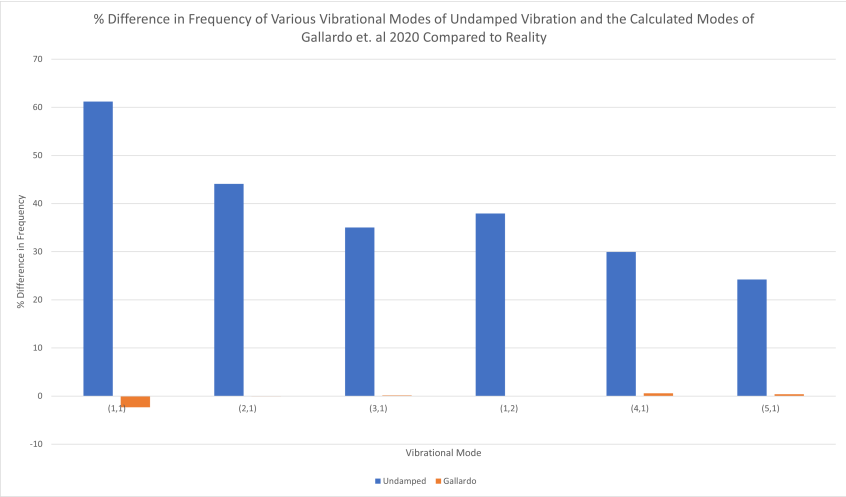

Figure 17. Percent Difference in Frequencies of Various Vibrational Modes of Undamped Vibration and the Calculated Modes of Gallardo et. al 2020 Compared to Reality

4 DISCUSSION

4.1 Effect of Initial Conditions, Damping and Viscoelastic Effects

The various models above attempted various approximations for the initial condition of the drum, and also considered some of the effects of a timpani that are not considered by the standard 2-dimensional wave equation.

When examining the frequencies and amplitudes and assessing the sounds resulting from each of these models, we are quickly able to see that the choice of approximating the initial conditions has a significant effect on the resulting sound and the animation of the resulting wave: imparting a initial velocity on only a small region centering around the point of impact leads to a highly unphysical and inaccurate animation. Using a initial displacement model such as plucked string leads to a more membrane-like vibration than the mallet, but nonetheless is inaccurate in several respects and also leads to an inaccurate sound, which demonstrates that despite using a similar class of partial different equation, a plucked string and vibrating drumhead are not perfectly analogous.

Imparting an instantaneous initial velocity from a flat membrane mirroring that of the membrane leads to a slightly more accurate sound and membrane animation than the two models above, but the vibration still does not exactly resemble membrane vibration.

Ascribing an initial force to the model (rather attempting to assume the velocity or displacement a priori), as was done conditions of the force models (assuming a flat stationary membrane and using a two-phase partial differential equation) gave a more realistic-looking vibration and a relatively more accurate sound, with the modified force model giving a more accurate sound than the model without viscoelasticity. However, the sound generated from this model is quite fuzzy - the initial impact is not immediately discernible.

Finally, incorporating a Dirac delta term into the forcing term had a drastic effect on the animation, periodogram and audio of the model - as the contribution (coefficient) of the Dirac term increased relative to the conical force term, the "fuzziness" that was inherent to the conical force term gets resolved into a clearer initial hit. In addition, the contributions of higher modes (that is, their amplitudes in the periodogram) are increased as the contribution of the Dirac term increases, with the most noticeable difference in the purely Dirac model.

Therefore, we observe overall that specifying an initial forcing term leads to the most realistic/physical results, as opposed to attempting to specify an initial shape or initial velocity a priori. In addition, it was found that while an extremely fine mesh (of nearly 8000 elements) was needed for the mallet radius model to produce results without significant noise, this mesh could be coarsened considerably and still produce realistic animations, periodograms and sounds for other models.

However, none of these initial conditions or forcing terms led to much significant change in the frequencies of each of the vibrational modes, meaning that all of them had the same pitch (approximately 111Hz, very close to an A2) despite their other qualitative differences. Rather, the resulting change in sound was due to the change in amplitudes of the various vibrational modes.

A small but discernible increase in frequency in the higher frequency modes (especially noticeable at (4,1) and above) was noticed in the PDE models that specified a viscoelastic term - this increase was typically on the order of 1-2 Hz (or about 0.2-0.6%), with larger increases noted for higher frequency modes. While perhaps numerically difficult to separate from the human error entailed by "Get Coordinates", this effect still cannot be ignored - it cannot regarded as pure coincidence that all the models with a viscoelastic term showed this subtle increase in the higher modes. Nonetheless, a change this small would have next to no impact on the sound.

Thus, we see that while damping is necessary for the vibration of the drum to fade, it seems to have little effect on the frequencies of the vibrational modes. In addition, while factoring in viscoelastic effects in the wave equation suppresses the higher frequency modes by nature of the Laplacian, which dampens high frequency vibrations faster, it also does not have a significant effect on the individual frequencies themselves, outside of small increases in frequency of the higher order modes.

4.2 Effect of the Point of Impact

In line with the overarching idea that "while changing initial conditions and forcing terms of the wave equation has little, if any, effect on the frequencies of vibrational modes, it may have a significant effect on the amplitude", we saw that changing the point of impact had next to no effect on the numerical frequencies of the vibrational modes (the difference between 0.75r and the alternative points of impact for any given mode did not exceed 0.2%), but it could have a significant effect on the amplitudes - in fact, it caused one of the higher frequency modes, (0,3), to be undetectable in the resulting periodograms.

It should be noted that the increased parity between the contributions of the higher frequency and lower frequency modes accomplished by increased the contribution of the Dirac term was counteracted by moving the point of impact closer to the center - in fact, while the normalized amplitude of all other modes relative to the fundamental (0,1) decreases the closer the point of impact is to the center, the biggest drops in amplitude are noted in the highest frequencies. This in turn also affected the sound somewhat: as the point of impact was moved closer to the center, the resolution of the initial impact decreased in clarity, with the sound becoming "fuzzier" once more like it had with a conical forcing term.

These results provide an interesting contrast to the results seen in Nishimura et. al 2018, which were tested on an air-loaded timpani - which demonstrated no significant change in the amplitudes of (1,1), (2,1)

and (3,1) at various points and in fact revealed an increase in amplitude for the (4,1) mode as the point of impact was moved closer to the center (Y. Nishimura and S. Nishimura 2015, p. 47) - from these findings, it seems that an air-loaded membrane is more tolerant to deviations in striking than a membrane that is not air-loaded, helping explain why there may be significant reported deviation in surveyed timpani players from the "ideal" of 0.75r reported by Rossing 1982.

4.3 Effect of Air Loading on the Vibration of the Membrane

The following version of the wave equation was used to model the vibration of a timpani (Gallardo et al. 2020, p. 7):

$$\rho u_{tt} = T\Delta(u + \frac{\partial u}{\partial t}) + P_- - P_+ \tag{49}$$

Given that c was specified as $\sqrt{T/\rho}$ in all of the models described prior, this means that the only difference in this model and the free vibration of the modified force model is the addition of the P_+ and P_- terms. These terms correspond to the acoustic pressure field both directly above and below the membrane of the timpani - in other words, it attempts to model the effect of air loading on the timpani, something that the models in the Methods section neglect.

This incorporation of air loading led to major improvements over the standard undamped model - while the % change in frequency between the undamped model and reality was often vast (ranging from 60% for the lower frequency modes to around 20% for the higher frequency modes), the error between Gallardo's observed model and the reality of the drum was nearly two orders of magnitude smaller. It is here that we also observe the disproportionate effect of air-loading on lower frequency modes: they seem to be affected significantly more than the higher frequency ones (Jones 2011), as seen by the much higher % error.

While it is likely that Gallardo et al. 2020 also modeled the impact force differently (as evidenced by their different choice of acceleration term, which used a cosine profile) (Gallardo et al. 2020, p. 9), previous discussion illustrates that that the forcing term does not seem to have a significant effect on the frequencies of the models. Therefore the primary reason that all modes explained above have significantly different frequencies for modes than both the calculated frequencies and the reality observed by Gallardo et al. 2020 is most likely that of air loading.

This large disparity in frequencies caused by air loading is corroborated by calculations done in Fletcher et. al 1997: with a kettle as specified similarly to Gallardo et al. 2020, significant drops in frequency were noted in all modes compared to an ideal membrane except for (0,1), which experienced a less significant

drop. Table 1 documents the frequencies of the (0,1) modes and the five modes that make up the harmonic frequency ratio in an air-loaded kettledrum ((1,1), (2,1), ..., (5,1)). (Fletcher and Rossing 1997, p. 590)

Mode	Ideal Membrane Frequency	Frequency with a Kettle
(0,1)	143	131
(1,1)	228	150
(2,1)	306	227
(3,1)	380	299
(4,1)	452	370
(5,1)	522	434

Table 1. Frequencies of "Harmonic" Vibrational Modes for Unloaded and Air-loaded Membranes

4.4 Future Steps - Accounting for Air Loading

Thus, it is clear that any accurate model of a drum must account for the effects of air loading. The most common approach in literature makes use of coupled systems where the vibration of the timpani drumhead is coupled with the acoustic pressure field inside and outside of a cylindrical kettle with length L and radius a. The origin is set to be at the center of the base of the drumhead (meaning that the

$$\sigma \frac{\partial^2 u}{\partial t^2} = T\nabla^2(u + \nu \frac{\partial u}{\partial t}) + P(\rho, \phi, L_-, t) - P(\rho, \phi, L_+, t) \tag{50}$$

where T and σ stand for tension and areal membrane density as usual, ν represents the viscoelastic coefficient, P is a function representing the acoustic pressure in a 3D space at the point (ρ, ϕ, z) in the cylindrical coordinate system at time t, and $P(\rho, \phi, L_-, t)$ and $P(\rho, \phi, L_+, t)$ represent the pressure just below and above the membrane, respectively (which was set at height L).

The acoustic pressure field both inside and outside can be represented by the 3-dimensional wave equation:

$$(\Delta - \frac{1}{c_a} \frac{\partial^2}{\partial t^2})p = 0 \tag{51}$$

where c_a is the speed of light, and where the inner and outer pressure have different boundary conditions that are based on the assumption that the kettle walls act as a sound baffle (which sets restrictions on the pressure field inside the timpani), and that the outside pressure is also limited by a rigid and infinite baffle on the plane of the membrane.

Then, based on these assumptions, Fletcher et. al 1997 specifies that the pressure inside the kettle has

the boundary conditions

$$\frac{\partial p}{\partial \rho}(a, \phi, z, t) = 0 \tag{52}$$

$$\frac{\partial p}{\partial z}(\rho, \phi, 0, t) = 0 \tag{53}$$

Similarly, the pressure outside the kettle has the boundary condition of

$$\frac{\partial p}{\partial \rho}(\rho, \phi, L, t) = 0 \tag{54}$$

Factoring in the vibration generates a coupled system where the vibration of the membrane affects the air pressure just above and below the membrane, and where this air pressure differential can similarly affect the vibration of the membrane. This coupled system is typically solved (as done by both Gallardo et. al 2020 and Fletcher et. al 1997) through a Green's function approach: in both cases the Green's function was found for both the acoustic pressure field inside and outside of the membrane, which could then be factored into membrane vibration to determine the new air-loaded frequencies by iteratively solving an eigenvalue-eigenvector problem (Gallardo et al. 2020, pp. 8–9)

4.5 Near-harmonic ratios in an unloaded membrane

Interestingly, despite these often large disparities in frequencies between modes, it was noted that the pitch of the synthesized sound still matched that of the "real" drum recording, which was especially apparent in the more refined models, and that the sound was still quite harmonic in these refined models as well.

When examining the ratios between the frequencies of different vibrational modes, it was found that even in a membrane that is not loaded with air, a near-harmonic 2:3:4:5:6 frequency ratio can still be observed with specific modes. However, in this case, this ratio comes not from the (1,1),..., (5,1) modes as described by Rossing et. al 1982, but from the (0,1), (1,1) (2,1), (3,1), and (1,2) modes - moreover, given the relevant conditions specified by Gallardo et. al, the frequencies of these unloaded near-harmonic vibrational modes closely match to that of the air-loaded harmonic vibrational modes in a real drum - as Table 2 shows, the difference between the frequencies is surprisingly small - with some correspondences being nearly dead-on while the most significant deviations are still under 10%.

While these modes are still rather harmonic, as reflected by the synthesized sounds and in their only slight deviation from the harmonic modes of air loading, loading is still preferable because of the nature

"Harmonic" Mode	Unloaded	Air-Loaded	% Difference
(0,1) vs (1,1)	111.743	110.452	1.16883352
(1,1) vs (2,1)	178.044	165.581	7.526829769
(2,1) vs (3,1)	238.632	219.538	8.697355355
(3,1) vs (4,1)	296.461	271.299	9.274637946
(1,2) vs (5,1)	325.987	323.727	0.698119094

Table 2. % Difference in Frequencies of Near-Harmonic Ratios in Unloaded and Air-Loaded models.

of vibration of each of these modes: As Russell 2018 points out, the (0,1) mode radiates sounds very well, quickly transferring its vibrational energy into sound energy and dissipating quickly, leading to a sharp "thump" sound with no definite pitch - having the fundamental frequency be a mode that quickly dissipates is not ideal for a drum, and air-loading adjusts the frequencies so that modes that can contribute more to a pitch of a drum can be aligned properly.

4.6 Other Future Steps

While accounting for air-loading will most likely encompass the most significant improvement to the model, it may be possible to also factor in the other effects mentioned in the Introduction not accounted for either by the standard wave equation or the models mentioned here, such as the effect of bending stiffness resulting from the membrane not being perfectly elastic, or exploring how to model nonvertical vibrations.

In addition, once the model is sufficiently refined, we can further explore the interpersonal and intrapersonal variation between points of impact - if we can obtain more survey results from players of other orchestras, we can use the methods of density estimation to better craft an overall distribution that models the points of impact across all timpani players. In addition, for a specific timpanist, we can gauge the points of impact that result from several repeated trials, and construct a distribution of "intrapersonal variability" - the variation inherent to a person striking the drum repeatedly.

In the context of digital music composition, this can be used in incorporating human variability into a piece of music - for any given of piece, the former "interpersonal distribution" can be sampled to determine a specific "timpanist" for the entire piece of music, and then incorporate the intrapersonal variability distribution to that timpanist between individual uses of the drum instrument throughout the piece.

Finally, while the base NDSolveValue method present in Mathematica (which took 3-5 minutes to run for meshes with 200 triangles) was adequate for the exploratory purposes of this thesis and its flexibility appreciated in exploring a wide range of models, use of similar computations in the context of music composition (which would require much faster computations on the scale of seconds or less) would require refinements to the method for faster or more accurate computation, such as having more control over where mesh elements are located (like having them more concentrated around the point of impact, rather

than using an automatically generated mesh by Mathematica) or various other optimizations that could be specified ahead of time in the code itself, rather than leaving those components up to an on-demand solver.

5 APPENDICES

5.1 Appendix A: Meshes

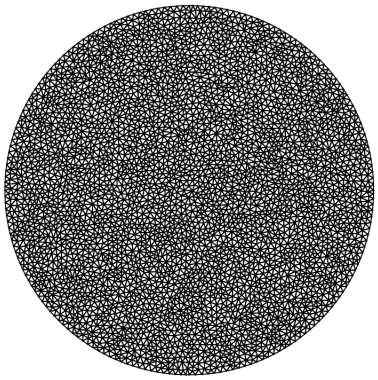

Figure 18. Mesh used for the mallet radius model

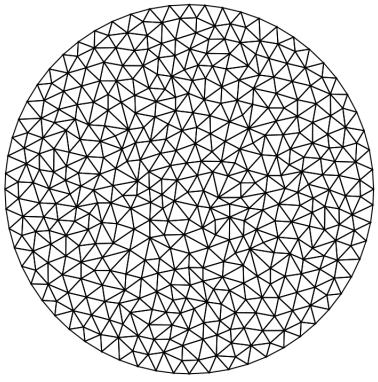

Figure 19. Mesh used for the initial displacement and initial velocity models

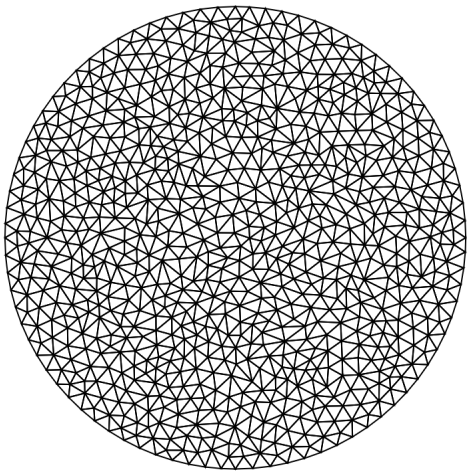

Figure 20. Mesh used for the forced phase of all forced models

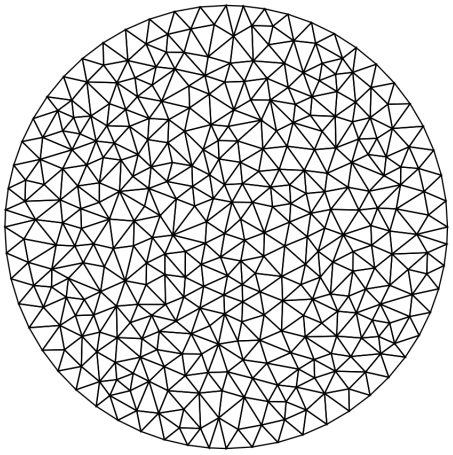

Figure 21. Mesh used for the free phase of the forced model

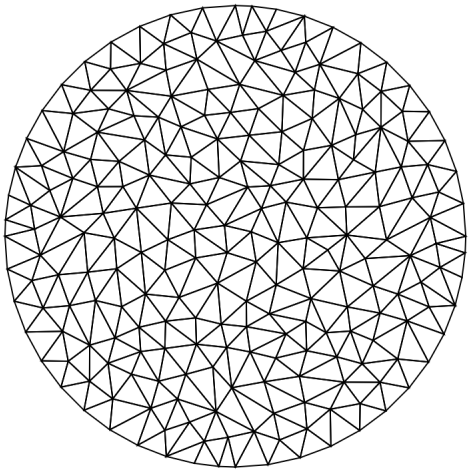

Figure 22. Mesh used for the free phase of the modified forced model

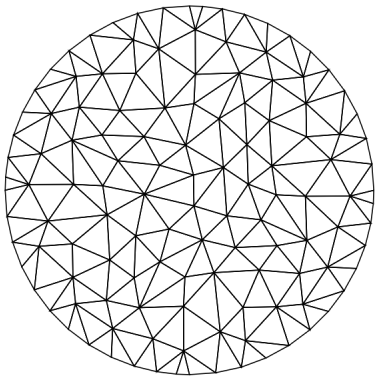

Figure 23. Mesh used for the free phase of the Dirac modified forced model

5.2 Appendix B: Selected Animation Frames

NOTE: These animation frames are simply provide one snapshot of the model at a specific point in time and can only provide a preview of the actual nature of the observed vibration. For that reason, animations are included in the supplementing PowerPoint on slides 20 (purely Dirac at 0.75r), slide 21 (purely Dirac at alternative points of impact), and slides 44-46 (for all remaining models).

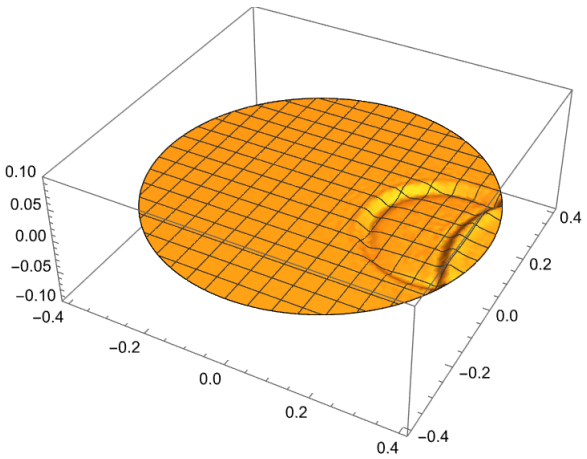

Figure 24. The Mallet Radius Model

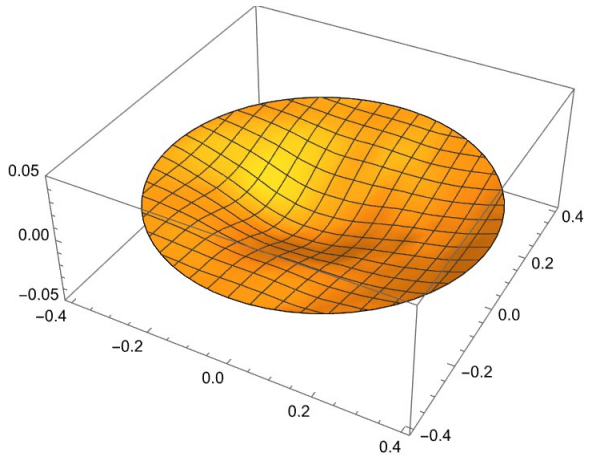

Figure 25. The Initial Displacement Model

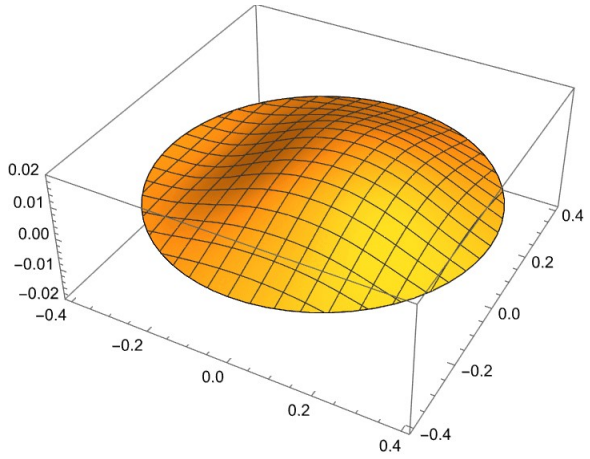

Figure 26. The Velocity Model

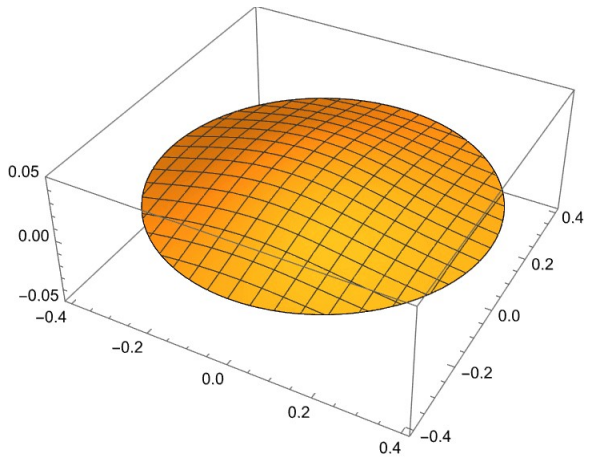

Figure 27. The Forced Model

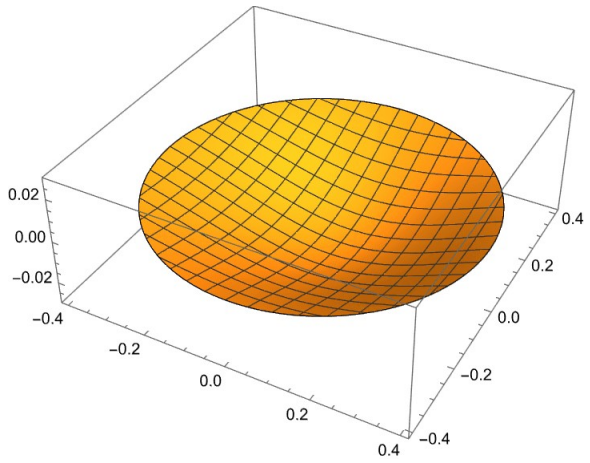

Figure 28. The Modified Forced Model

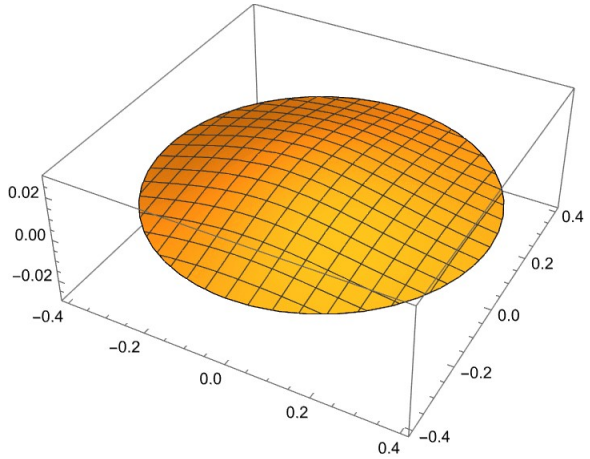

Figure 29. The Modified Forced Model with mostly conical forcing term

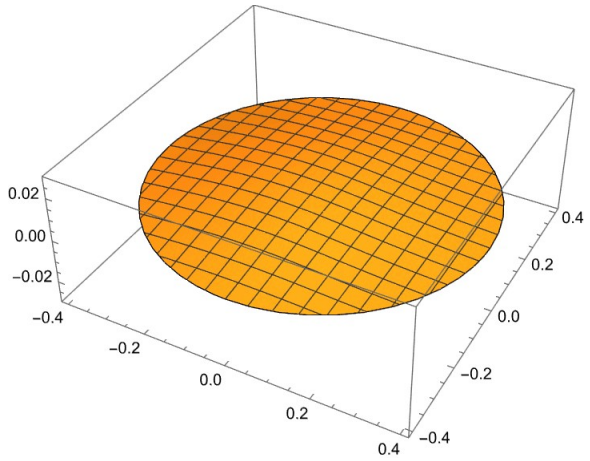

Figure 30. The Modified Forced Model with mostly Dirac forcing term

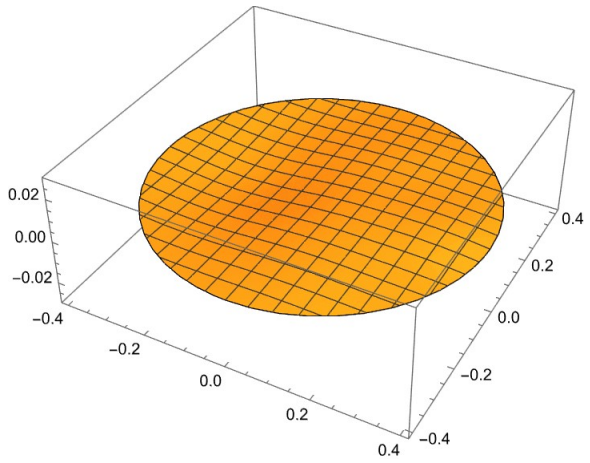

Figure 31. The Modified Forced Model with purely Dirac forcing term

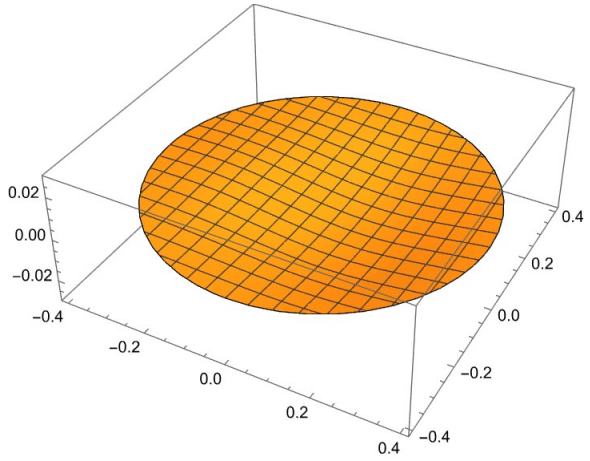

Figure 32. The Modified Forced Model with purely Dirac forcing term with point of impact 0.642r

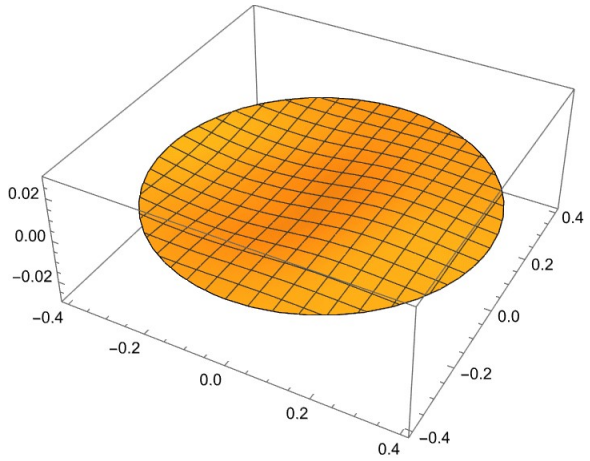

Figure 33. The Modified Forced Model with purely Dirac forcing term with point of impact 0.425r

5.3 Appendix C: Periodograms

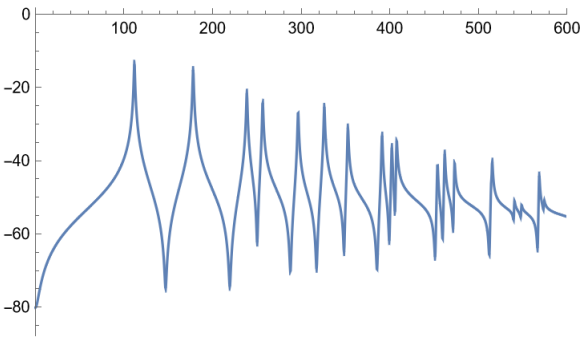

Figure 34. Periodogram of the initial displacement model

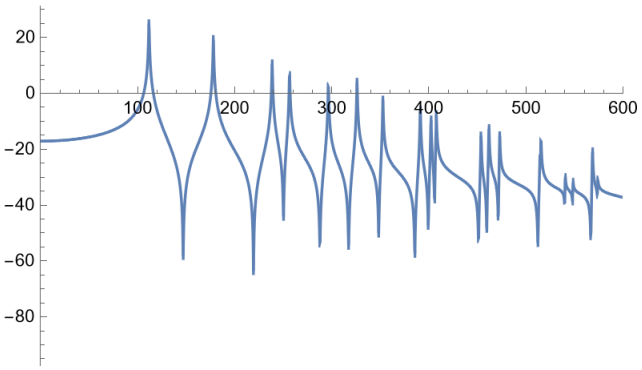

Figure 35. Periodogram of the initial velocity model

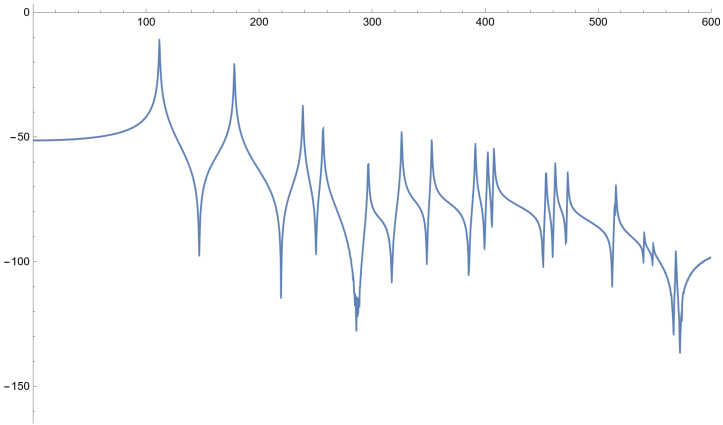

Figure 36. Periodogram of the forced model

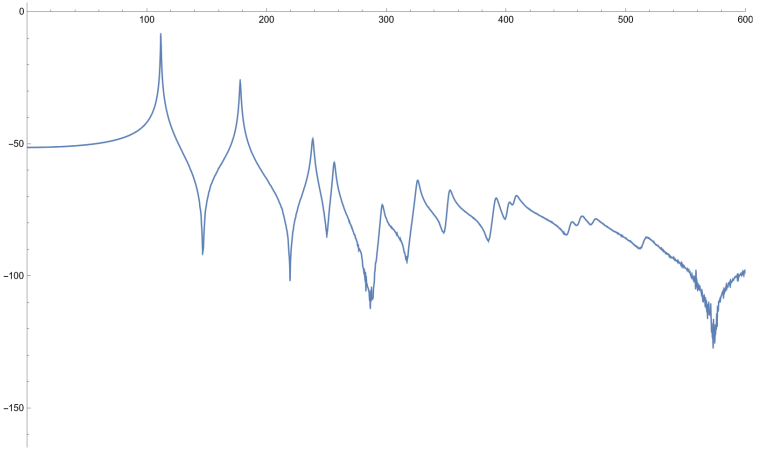

Figure 37. Periodogram of the modified forced model

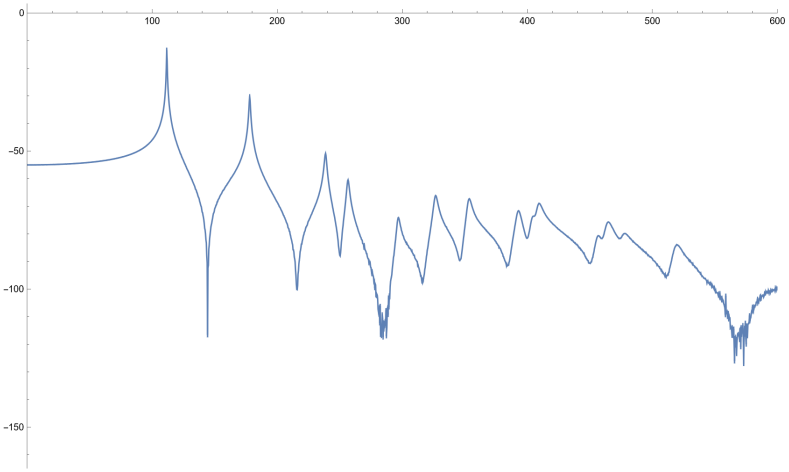

Figure 38. Periodogram of the modified forced model with a mostly conical forcing term

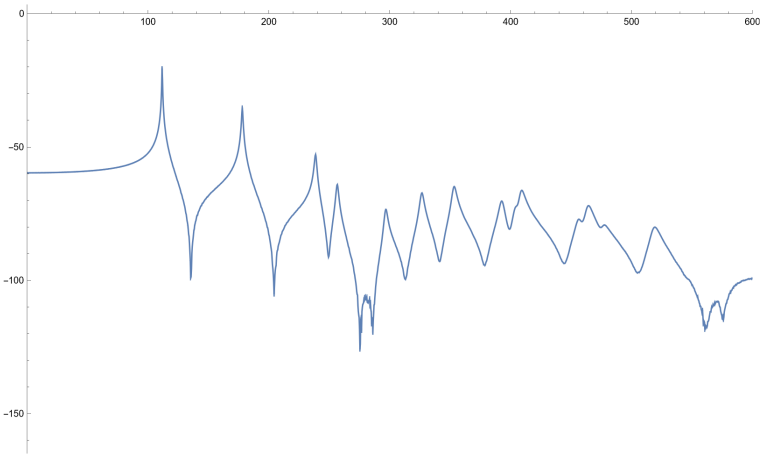

Figure 39. Periodogram of the modified forced model with a mostly Dirac forcing term

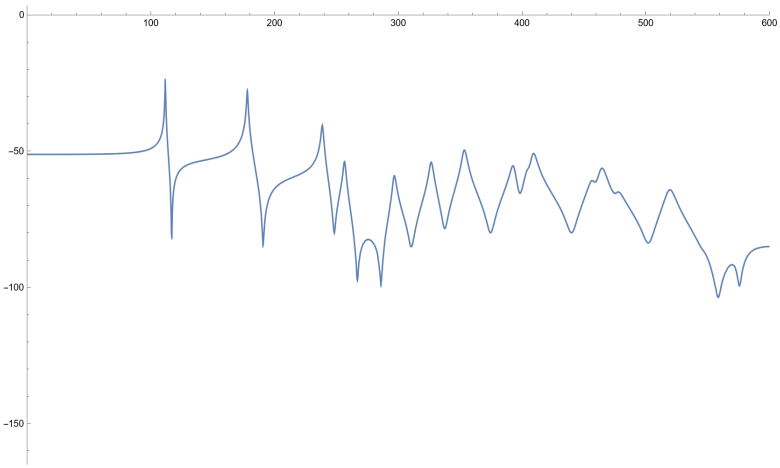

Figure 40. Periodogram of the modified forced model with a purely Dirac forcing term

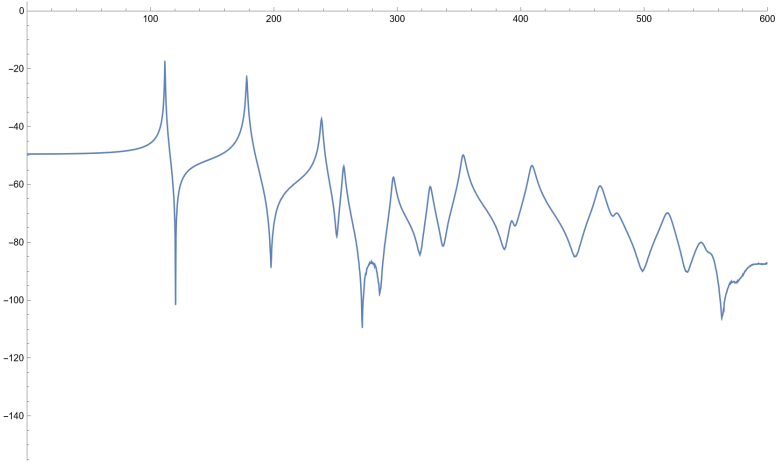

Figure 41. Periodogram of the purely Dirac modified forced model with a point of impact of 0.642r

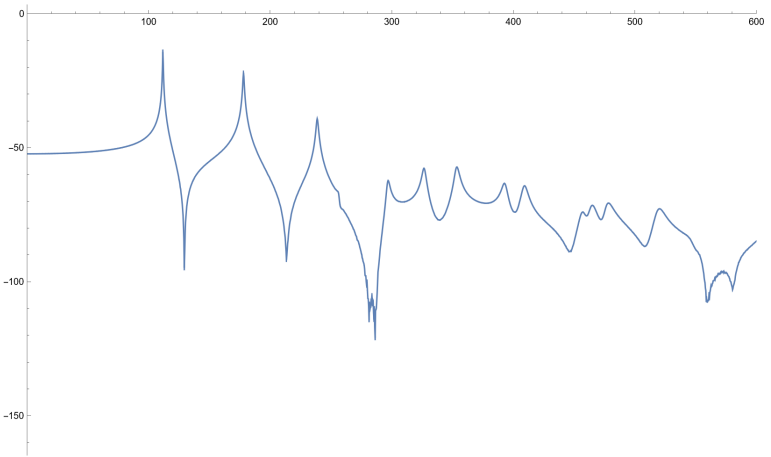

Figure 42. Periodogram of the purely Dirac modified forced model with a point of impact of 0.425r

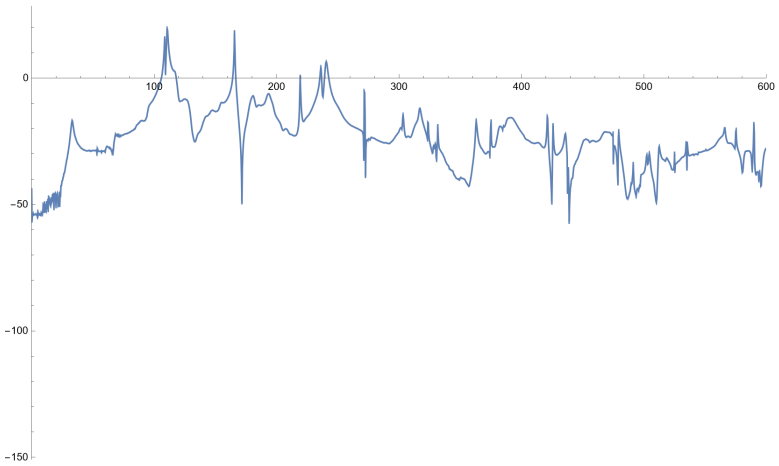

Figure 43. Periodogram of the real recorded sound

5.4 Appendix D: Audio Waveforms

NOTE: These audio waveforms only provide the amplitude of the sound at any given time and can only provide a preview of the actual nature of the observed sound: for that reason, the audio for each of the synthesized sounds can be found in the supplementing PowerPoint presentation on slide 26 (for the purely Dirac model at 0.75r), slide 27 (for the purely Dirac model at different points of impact), and slide 47 (for all remaining models)

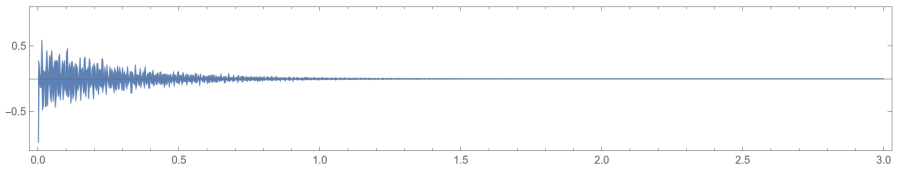

Figure 44. Initial Displacement Model

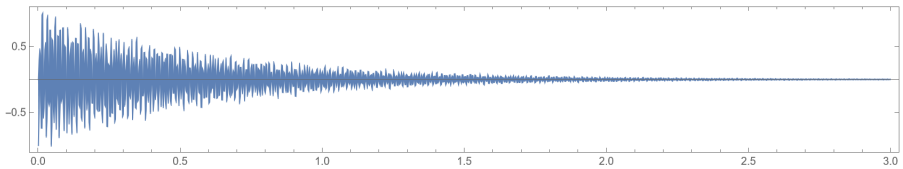

Figure 45. Initial Velocity Model

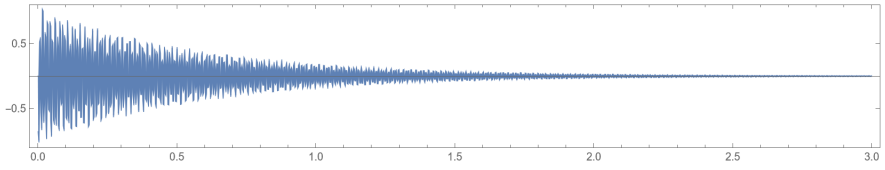

Figure 46. Forced Model

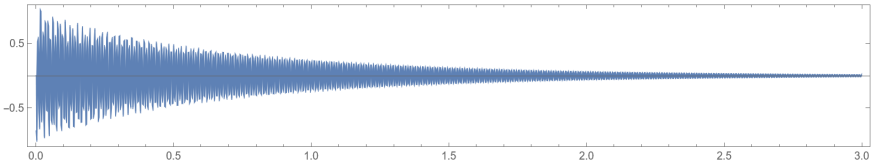

Figure 47. Modified Forced Model

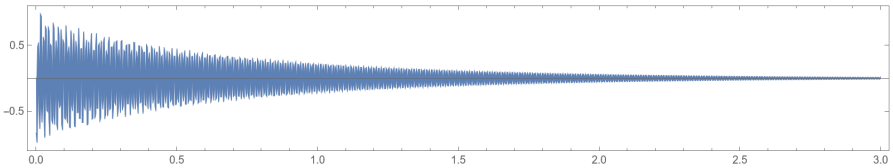

Figure 48. Modified Forced Model with mostly conical forcing term

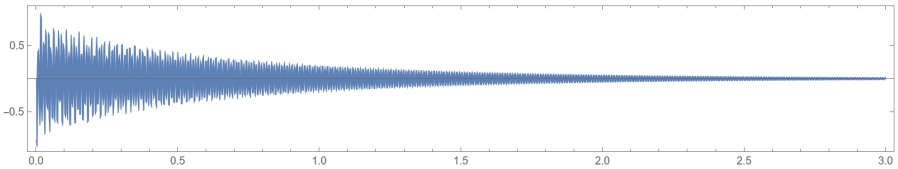

Figure 49. Modified Forced Model with mostly Dirac forcing term

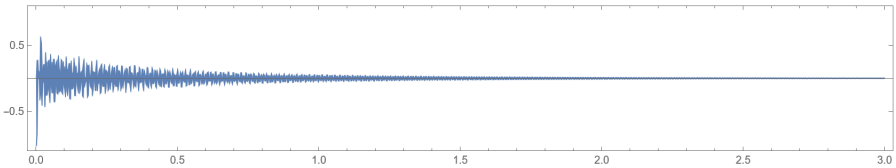

Figure 50. Modified Forced Model with purely Dirac forcing term

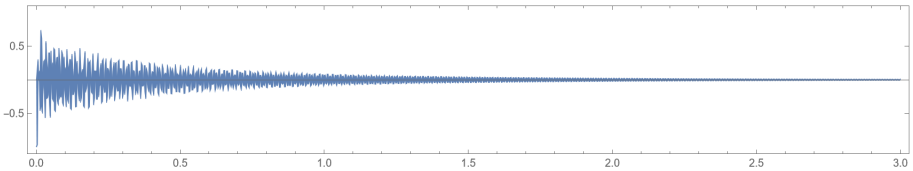

Figure 51. Purely Dirac Modified Forced Model with point of impact 0.642r

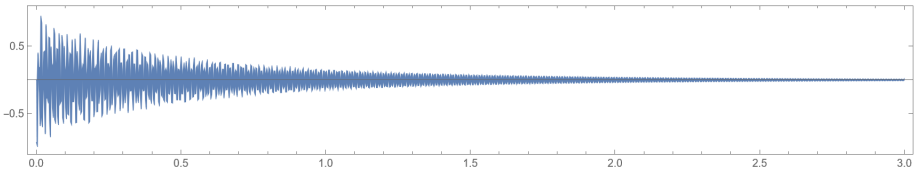

Figure 52. Purely Dirac Modified Forced Model with point of impact 0.425r

5.5 Appendix E: Frequency Raw Data

Mode	UD	ID	IV	Forced	Forced + Viscoelasticity	Gallardo Air Loading	Reality
(0,1)	111.743	111.749	111.38	111.732	111.63	not stated	not stated
(1,1)	178.044	177.931	177.925	178.118	177.974	107.9	110.452
(2,1)	238.632	238.754	238.637	238.705	238.641	165.4	165.581
(0,2)	256.947	256.698	256.4	256.679	256.735	not stated	not stated
(3,1)	296.461	296.547	296.168	296.493	296.47	219.8	219.538
(1,2)	325.987	325.91	325.861	325.963	326.271	236.4	236.305
(4,1)	352.601	352.709	352.639	352.633	353.234	272.8	271.299
(2,2)	391.117	391.16	391.346	391.189	391.905	not stated	not stated
(0,3)	402.105	402.113	402.216	402.205	402.904	not stated	not stated
(5,1)	407.577	407.706	407.783	408.802	408.935	325	323.727

Table 3. Table of raw frequencies of various vibrational mode obtained through the results of Gallardo et. al 2020 or from "Get Coordinates" on the periodograms of various models and reality. "UD" means the theoretical undamped frequencies from the normal 2D wave equation, "ID" means the initial displacement model, and "IV" means the initial velocity model.

Mode	Mostly Conical	Mostly Dirac	Purely Dirac
(0,1)	111.6	111.774	111.64
(1,1)	177.947	178.06	177.914
(2,1)	238.472	238.697	238.668
(0,2)	256.406	256.53	256.691
(3,1)	296.576	296.957	297.097
(1,2)	326.645	326.682	326.457
(4,1)	353.546	353.433	353.491
(2,2)	393.149	392.67	392.734
(0,3)	404.606	403.965	404.362
(5,1)	409.09	409.31	409.594

Table 4. Table of raw frequencies obtained through "Get Coordinates" on the periodograms of the purely Dirac models with different forcing terms.

Mode	0.642r	0.425r
(0,1)	111.564	111.569
(1,1)	177.757	178.148
(2,1)	238.277	238.514
(0,2)	256.433	256.268
(3,1)	296.786	297.104
(1,2)	326.784	326.399
(4,1)	353.578	353.623
(2,2)	392.895	392.683
(0,3)	UNDETECTABLE	UNDETECTABLE
(5,1)	409.865	409.254

Table 5. Table of raw frequencies obtained through "Get Coordinates" on the periodograms of the purely Dirac models with different points of impact. Note that since there was no distinct peak to be found at the (0,3) frequency range, there is no way to discern its exact frequency.

5.6 Appendix F: Amplitude Raw Data

Mode	Initial Displacement	Initial Velocity	Forced	Forced + Viscoelasticity
(0,1)	-13.09	25.33	-10.7	-8.45
(1,1)	-14.57	19.55	-20.39	-25.85
(2,1)	-20.76	11.01	-37.44	-47.75
(0,2)	-23.7191	6.48	-46.59	-56.92
(3,1)	-26.86	2.84	-60.94	-72.55
(1,2)	-24.92	4.1	-47.8	-64.01
(4,1)	-30.28	-2.3	-51.26	-67.56
(2,2)	-32.86	-6.07	-52.69	-70.45
(0,3)	-35.82	-8.96	-53.92	-71.9
(5,1)	-34.71	-6.95	-54.66	-69.32

Table 6. Table of raw amplitudes of various vibrational modes (before normalization) obtained through "Get Coordinates" on the periodograms of the various models.

Mode	Mostly Conical	Mostly Dirac	Purely Dirac
(0,1)	-12.28	-19.62	-23.59
(1,1)	-29.45	-34.46	-27.28
(2,1)	-50.37	-52.27	-40.34
(0,2)	-60.09	-63.74	-53.67
(3,1)	-73.99	-73.18	-59.07
(1,2)	-65.97	-66.84	-54.2
(4,1)	-67.1	-64.41	-49.58
(2,2)	-71.39	-70.08	-55.3893
(0,3)	-73.32	-72.24	-56.7
(5,1)	-68.91	-65.9	-50.77

Table 7. Table of raw amplitudes of various vibrational modes (before normalization) obtained through "Get Coordinates" on the periodograms of modified forced models with different forcing terms.

Mode	0.642r	0.425r
(0,1)	-17.09	-13.16
(1,1)	-22.2	-21.22
(2,1)	-36.65	-38.27
(0,2)	-53.59	-65.93
(3,1)	-57.33	-61.77
(1,2)	-60.57	-57.21
(4,1)	-49.48	-56.94
(2,2)	-72.28	-62.85
(0,3)	UNDETECTABLE	UNDETECTABLE
(5,1)	-53.47	-63.79

Table 8. Table of raw amplitudes of various vibrational modes (before normalization) obtained through "Get Coordinates" on the periodograms of the purely Dirac modified forced model with various points of impact. Note that since there was no distinct peak to be found at the (0,3) frequency range, there is no way to discern its exact amplitude.

5.7 Appendix G: Bessel Function Plots

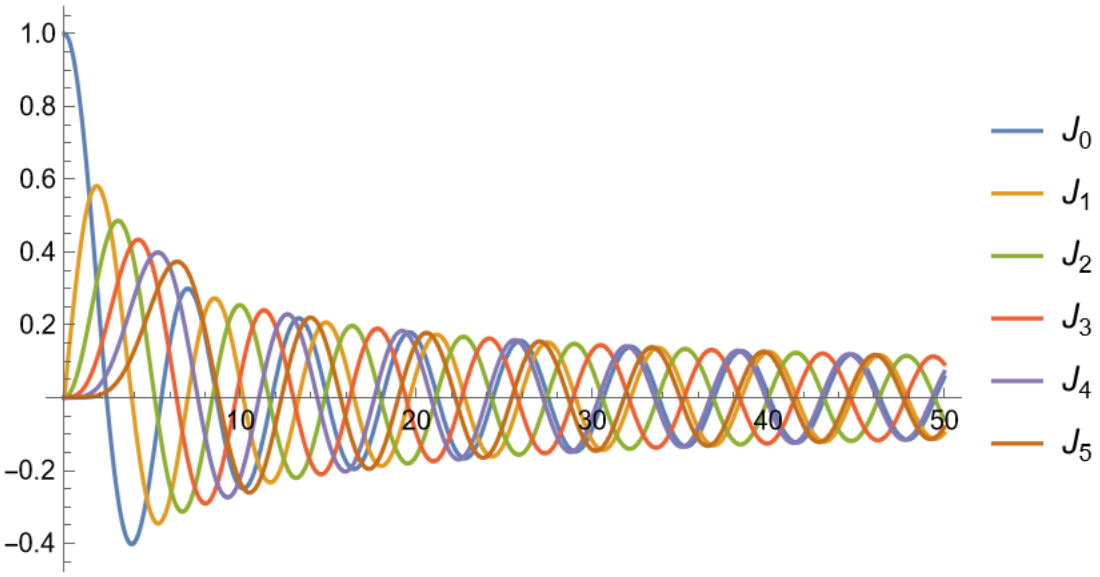

Figure 53. Bessel functions of the first kind J_n for $n = 0, 1, 2, 3, 4, 5$.

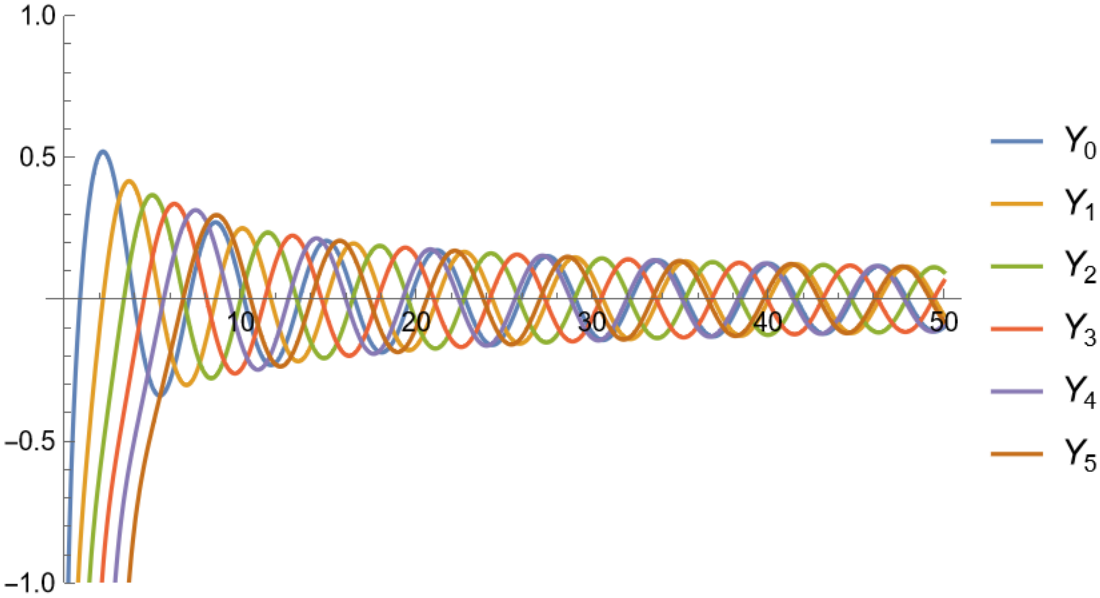

Figure 54. Bessel functions of the first kind Y_n for $n = 0, 1, 2, 3, 4, 5$. Note how there is always a singularity at $x = 0$.

PRINTED REFERENCES

Borthwick, David (2017). "Introduction to Partial Differential Equations". In: 2nd ed. New York: Springer. Chap. 4.

Fletcher, Neville and Thomas Rossing (1997). "The Physics of Musical Instruments". In: 2nd ed. New York: Springer. Chap. 18.

Gallardo, Erik et al. (2020). "Sound model of an orchestral kettledrum considering viscoelastic effects". In: *Applied Acoustics* 164, Article 107284.

Jones, Richard (2011). "The Well-Tempered Timpani: In Search of the Missing Fundamental". In: 2nd ed. https://wtt.pauken.org/chapter-3/air-loading-2. Timpani Analytic International. Chap. 3.

Nishimura, Yuya and Sohei Nishimura (2015). "Acoustic Analysis of Timpani: Specific Mode by Striking Point". In: *International Journal of Emerging Engineering Research and Technology* 3.10, pp. 44–47.

Rossing, Thomas (1982). "The Physics of Kettledrums". In: *Scientific American* 247.5, pp. 172–179.

Wagner, Andreas (2006). "Analysis of Drumbeats – Interaction between Drummer, Drumstick and Instrument". MA thesis. KTH Royal Institute of Technology.

Wang, Yanghua (2016). "Generalized viscoelastic wave equation". In: *Geophysical Journal International* 204.2, pp. 1216–1221.

NON-PRINTED RESOURCES

Daileda, Ryan (2012). *More on the Circular Membrane Problem*. http://ramanujan.math.trinity.edu/rdaileda/teach/s12/m3357/lectures/lecture_4_3_short.pdf. Last accessed 10 March 2022.

Haber, Howard (2009). *Solving the Simple Harmonic Oscillator*. http://scipp.ucsc.edu/~haber/ph5B/sho09.pdf. Last accessed 10 March 2022.

Ham, David and Colin Cotter (2014). *Convergence of finite element approximations*. https://finite-element.github.io/L5_convergence.html. Last accessed 10 March 2022.

Kréemes, Khr1spy (2019). *F-sharp Timpani in (Slo-Mo)*. https://www.youtube.com/watch?v=dg1YRlBnbTs. Last accessed 12 March 2022.

Müller, Meinard (n.d.). *Intervals*. https://www.audiolabs-erlangen.de/resources/MIR/FMP/C5/C5S1_Intervals.html. Last accessed 10 March 2022.

Nagata, Wayne (2014). *Vibrating Circular Membrane*. https://personal.math.ubc.ca/~nagata/sci1/drum.pdf. Last accessed 9 March 2022.

Russell, Dan (2020). *The Plucked Fixed-Fixed String*. https://www.acs.psu.edu/drussell/Demos/Pluck-Fourier/Pluck-Fourier.html. Last accessed 12 March 2022.

— (2018). *Vibrational Modes of a Circular Membrane*. https://www.acs.psu.edu/drussell/demos/membranecircle/circle.html. Last accessed 10 March 2022.

Weisstein, Eric (n.d.). *Complete Orthogonal System*. https://mathworld.wolfram.com/CompleteOrthogonalSystem.html. Last accessed 10 March 2022.

Yong, Darryl (n.d.). *Lecture 14: Playing the Timpani: Vibrations of a circular membrane*. https://www.math.hmc.edu/~ajb/PCMI/lecture14.pdf. Last accessed 10 March 2022.